Electronic Supplementary Material (ESI) for ChemComm.

# Supporting Information

## Stabilization and Activation of Polyoxometalate over Poly(vinyl butylimidazolium) cation towards Electrocatalytic Water Oxidation in Alkaline Media

Ganga Singh, Subhasis D. Adhikary and Debaprasad Mandal*

Department of Chemistry, Indian Institute of Technology Ropar, Rupnagar, Punjab 140001, India

### Physical measurements

FT-IR spectra were recorded in the range of 400−4000 cm$^{-1}$ using Shimadzu spectrometer with a spectral resolution of 4 cm$^{-1}$ and 100 scans. UV-vis. spectra were recorded in Shimadzu (UV-2600) spectrophotometer. NMR spectra were recorded on a Jeol JNM ECS 400 MHz NMR spectrometer at 293 K in 5 mm o.d. tube. Powder X-ray diffraction (P-XRD) patterns were recorded in Rigaku Miniflex III diffractometer. Gas chromatographic analysis was performed in Shimadzu gas chromatograph GC-2010 Plus with CP-Molsieve 5Å (25m x 0.32 mm x 30 μm) column fitted to thermal conductivity detector (TCD). The retention time for oxygen was 2.89 min. and that of nitrogen 3.95 min.

Single crystal X-ray data were collected using graphite monochromated Mo Kα radiation (λ = 0.71073 Å) on a Bruker D8 SMART APEX2 CMOS diffractometer at 300 K. Data integration was performed using SAINT. Routine Lorentz and polarization corrections were applied and empirical absorption corrections were performed using SADABS. SIR97 were used to solve the structure and the refinement was performed using SHELXL2013**.** The crystal data of $Na_{12}[Co\text{-}WCo_3]$ was matched with the previously reported data of our group (CCDC no. 1558372).[1]

Thermogravimetric analysis (TGA) was performed in a TGA/DSC 1 instrument with an SDTA sensor (Mettler-Toledo). Thermal data were analyzed in STARe software. The temperature, weight and tau lag was calibrated using an aluminium/zinc standard sample. To avoid external atmosphere effects, high-purity nitrogen gas (99.99%) was passed over the sample at a flow rate of 40 mL min$^{-1}$ throughout the experiment. The experiments were performed using an alumina pan as a sample holder. Thermal stability was performed by heating the sample from 25 °C to 800 °C at a rate of 10 °C/min.

## Electrochemical studies

### Sample preparation and electrochemical investigations

Electrochemical analysis was carried out in a single compartment three-electrode electrochemical cell set-up. The glassy carbon (GC, Ø3 mm) electrode was employed as working electrode hosting the catalyst and was referenced against Hg/HgO/1 M KOH with a Pt-mesh counter electrode. The GC working electrode was polished to a mirror finish before analysis using alumina slurry of various grades ranging from 3 to 0.05 µm over the Nylon polishing cloth (SM 407052, AKPOLISH). The GC electrode was further ultrasonicated in deionized water for 15 min to remove any alumina particles sticking over the surface following which it was rinsed thoroughly. Catalyst slurry was prepared by dispersing fine particles of the composite powder (1.25 mg) in a mixture of isopropyl alcohol (IPA, 20 µL) and deionized water (480 µL) and further sonicated for 30-40 minute before coating 20 µL slurry (50 µg) over polished GC electrode (Ø3 mm).

The electrochemical experiments were performed using Bio-Logic (VSP 300). Electrocatalytic activity composites toward electrocatalytic water oxidation was performed in deaerated 1 M KOH electrolyte (pH 14) or in 0.4 M sodium phosphate (NaPi) buffer of pH 8 at a scan rate of 50 mV/s. Cyclic voltammogram of [PVIM][Co-$WCo_3$] composite was also performed at a scan rate of 5 mV/s in both pH 8 and pH 14.

## Syntheses of POMs and POM-based composites

### Synthesis of $Na_{12}[WCo_3(H_2O)_2(CoW_9O_{34})_2]$. {$Na_{12}$[Co-$WCo_3$]}

The synthesis of $Na_{12}$[Co-$WCo_3$] was performed under microwave heating (detail experimental parameters are given in Table S1).

The Teflon microwave vials was charged with a mixture of $Na_2WO_4.2H_2O$ (16.000 g, 48.48 mmol), 60 mL of $H_2O$ and 2 mL of conc. $HNO_3$ and microwave irradiated for 30 min at 80-85 °C. After cooling to room temperature, the solid $Co(NO_3)_2.6H_2O$ (3.656 g, 12.56 mmol) was added and further microwave irradiated for 30 minutes at 85-90 °C. The obtained hot solution was filtered and the filtrate was allowed for crystallization. After 2-3 days deep-green coloured needle shaped crystals were collected by filtration. The obtained crystals were recrystallized from water, and dried at ~80 °C under high vacuum to obtain the title compound $Na_{12}$[Co-$WCo_3$] (1.562 g, 48.38%). FT-IR ($cm^{-1}$): 1622, 1388, 916, 858, 684, 531.

| **Table S1. Microwave reaction parameters** | |
|---|---|
| Maximum power | 500 W |
| IR temperature limit | 95 °C |
| Internal temperature limit | 80 °C |
| Power ramp | 300 W for 5 minutes |
| Power hold | 300 W for 30 minutes |

### Synthesis of poly(1-vinylbutylimidazolium bromide) (PVIMBr)

Synthesis of PVIMBr was performed as follows, according to our previously reported procedure.[2]

**Poly(1-vinylimidazole) (1).** A Schlenk tube was charged with 1-vinylimidazole (0.941 g, 10.00 mmol), azobis-(isobutyronitrile) (1.0 wt.%, 0.013 g), and 4.0 mL of dry toluene. The mixture was degassed under vacuum using three freeze-thaw cycles, and the presence of oxygen, if any, was removed by argon purging for 30 min. The reaction mixture was heated at 70 °C for 24 h. The obtained solid was purified using diethyl ether and dried under vacuum to yield **1** as a white powder (0.750 g, 80%). The synthesized polymer is soluble in water and methanol but insoluble in chloroform, tetrahydrofuran, and toluene. $^1$H NMR ($D_2O$, δ ppm): 7.06-6.64 (broad, 3H, imidazole ring proton), 3.74-2.57 (broad, 1H), 2.12-1.9 (broad, 2H).

**Poly(1-vinylbutyl imidazolium bromide) [PVIM]Br (2).** A Schlenk tube fitted with a condenser was charged with poly(1-vinylimidazole) **1** (0.339 g, 3.62 mmol), n-butyl bromide (0.543 g, 3.98 mmol), and dry methanol. The reaction mixture was heated at 60 °C for 48 h and further added to acetone to obtain a precipitate of **2** (0.772 g, 92.3%). $^1$H NMR (DMSO-$d_6$, δ ppm): 9.61 (broad, 1H, NCHN), 7.83-7.73 (broad, 2H, NCHCHN), 4.12-3.84 (broad, 4H), 2.51-2.49 (broad, 2H), 1.84 (broad, 2H), 1.33 (broad, 2H), 0.94 (broad, 2H).

### Synthesis of [PVIM][Co-WCo$_3$]

[PVIM][Co-WCo$_3$] was prepared by ion-exchange metathesis. Na$_{12}$[Co-WCo$_3$] (0.155 g, 0.39 mmol) was dissolved in 10 mL of water in an RB flask to get a clear green solution and a solution of [PVIM]Br dissolved in 15 mL water was added slowly with stirring. Immediately, the clear solution becomes coagulated, which was heated to 80 °C for 2 h. The resultant emulsion suspension was cooled to room temperature and filtered through frit (the clear colourless filtrate indicates the formation of the desired conjugate). The precipitate was washed with water (3×10 mL) and dried at ∼70 °C under high vacuum to get greenish [PVIM][Co-WCo$_3$] (0.328 g, 83.3 wt%).

### Synthesis of ZIF-8

ZIF-8 was prepared by slightly modifying the literature procedure.[3] A round bottom flask was charged with 2-methyl imidazole (0.658 g, 8.00 mmol) and dissolved in 8 mL methanol. To the clear solution, a solution of $Zn(NO_3)_2.6H_2O$ (0.599 g, 2.00 mmol) in methanol (6 mL) was added slowly. The mixture was stirred for 1 h at room temperature and then kept undisturbed for 24 h. The obtained precipitate was filtered through frit, washed with methanol (15 mL) and dried at ~80 °C under vacuum to get ZIF-8 (0.125 g, 9.9 wt.% ). FT-IR (cm$^{-1}$): 421, 658, 668, 685, 693, 759, 953, 994, 1089, 1145, 1178, 1308, 1416, 1681, 2360, 2926.

### Synthesis of Co-$WCo_3$@ZIF-8 composite

A Teflon-lined stainless steel autoclave was charged with a mixture of 2-methyl imidazole (0.328 g, 4.00 mmol), $Zn(NO_3)_2.6H_2O$ (0.301 g, 1.00 mmol) and methanol (15 mL). 3 mL aqueous solution of $Na_{12}$[Co-$WCo_3$] (0.051 g, 0.01 mmol) was added to mixer. The resultant mixture was sealed and autoclaved at 100 °C for 24 h. After slow cooling to room temperature, the coagulated mixture was filtered, the residue was washed with water and methanol (15 mL of each) and dried at ~80 °C under vacuum to get Co-$WCo_3$@ZIF-8 (0.301 g, 44.3 %). FT-IR ($cm^{-1}$): 419, 675, 748, 850, 913, 994, 1107, 1143, 1179, 1308, 1352, 1421, 1568, 1624, 3129.

### Synthesis of $Cs_{12}[WCo_3(H_2O)_2(CoW_9O_{34})_2]$. {$Cs_{12}$[Co-$WCo_3$]}

A thick-wall glass tube was charged with $Na_{12}$[Co-$WCo_3$] (0.051 g, 0.01 mmol) and dissolved in 1 mL water. To the clear greenish solution, caesium fluoride (0.019 g, 0.13 mmol) was added and the solution becomes coagulated. After 2 h stirring at room temperature, the solution was filtered. The solid residue was washed with water and dried at 70 °C under high vacuum to get $Cs_{12}$[Co-$WCo_3$] (0.025 g, 30.0 %). FT-IR ($cm^{-1}$): 533, 683, 720, 853, 910.

### Synthesis of $(C_{25}H_{54}N)_{12}[WCo_3(H_2O)_2(CoW_9O_{34})_2]$. {$(C_{25}H_{54}N)_{12}$[Co-$WCo_3$], $C_{25}H_{54}N$; aliquat-336 cation}

A thick-wall glass tube was charged with $Na_{12}$[Co-$WCo_3$] (0.050 g, 0.01 mmol) and dissolved in 1 mL water. To the clear greenish solution, 1 mL 1,2-dichloroethane solution of Aliquat-336 (0.052 g, 0.13 mmol) was added and stirred for 2 h at room temperature. The crude reaction mixture was then extracted with 1,2-dichloroethane and the organic solvent was evaporated. The obtained greenish viscous solid was dried at 70 °C under vacuum for 1 h to obtain $(C_{25}H_{54}N)_{12}$[Co-$WCo_3$] (0.085 g, 91.0%). FT-IR ($cm^{-1}$): 436, 539, 710, 748, 797, 867, 927, 1374, 1460, 2852, 2921, 2953.

### Synthesis of $K_{10}[Co_4(H_2O)_2(PW_9O_{34})_2]$. {$K_{10}$[P-$Co_4$]}

$K_{10}$[P-$Co_4$] was synthesized slightly modifying the literature procedure.[4] In a 100 mL two neck round bottom flask $Na_2WO_4.2H_2O$ (5.090 g, 15.39 mmol), $Na_2HPO_4.2H_2O$ (0.307 g, 1.71 mmol) and $Co(OAc)_2.4H_2O$ (0.851 g, 3.42 mmol) was taken and 35 mL water was added to it. The pH of the solution was adjusted from 9 to 7 (pH was ~8) by adding 6 N HCl. The purple suspension was then refluxed for 2 h and filtered. The filtrate was saturated by using solid KCl. Volume of solution was reduced and kept for crystallization. Purple crystals were obtained after 4 h. The crystals were collected by filtration and quickly washed with water and air dried to obtain $K_{10}$[P-$Co_4$] (0.729 g, 15%). **$^{31}$P-NMR** (ppm): 1883.69; **FT-IR** ($cm^{-1}$): 1031, 938, 875, 708. **Raman** (in solid), $cm^{-1}$: 231, 352, 509, 817, 899, 967, 1052.

## Synthesis of [PVIM][P-$Co_4$] composite

Poly(1-vinylbutylimidazolium bromide) (0.125 g, 0.59 mmol) was dissolved in 20 mL of water. To that solution, a solution of $K_{10}$[P-$Co_4$] (0.300 g, 0.05 mmol) dissolved in 8 mL water was added dropwise. After addition the solution becomes coagulated, which was heated at ~70 °C for 2 h. Coagulated compound was separated by filtration using fine porosity frit, washed with water and dried under vacuum at ~80 °C for 8 h to give the grey coloured composite (0.269 g, 63.2%).

## DFT Study

The geometries of POMs were fully optimized using Gaussian 09 program including solvent effects of CPCM model with water as a solvent. B3LYP theory was used with Hay-Wadt effective core potentials (ECPs) associated with the Lanl2dz basis set for tungsten, cobalt and the standard 6-31G+(d,p) basis set for all other atoms.

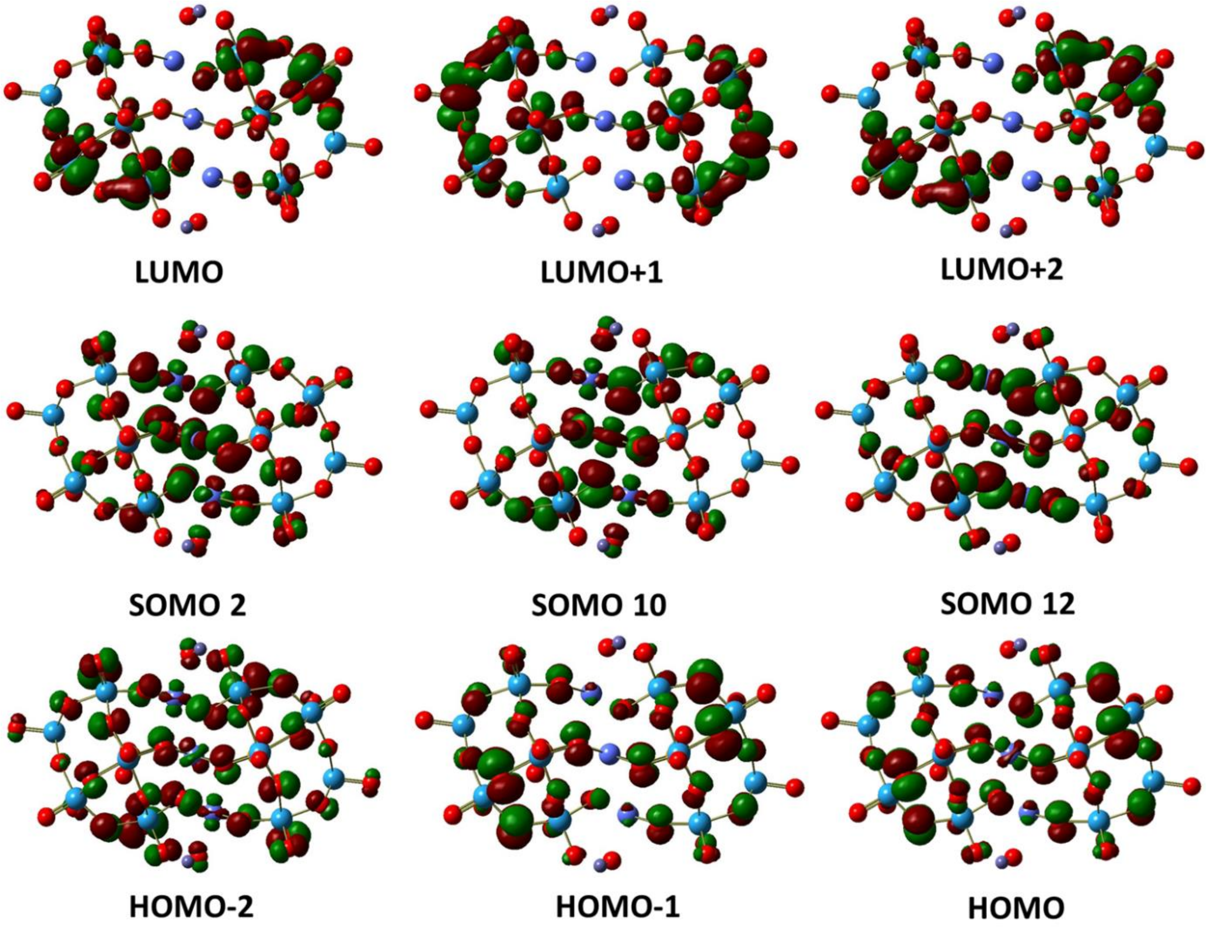

**Figure S1.** Frontier orbitals along with some important SOMOs of [P-$Co_4$] POM ($E_{HOMO}$ = -7.07 eV, $E_{LUMO}$ = -2.31 eV, $\Delta E$ = 4.76 eV, $E_{SOMO12}$ = -6.50 eV, $\Delta E_1$ = 4.19 eV where $\Delta E = E_{LUMO}-E_{HOMO}$ and $\Delta E1 = E_{LUMO}-E_{SOMO12}$)

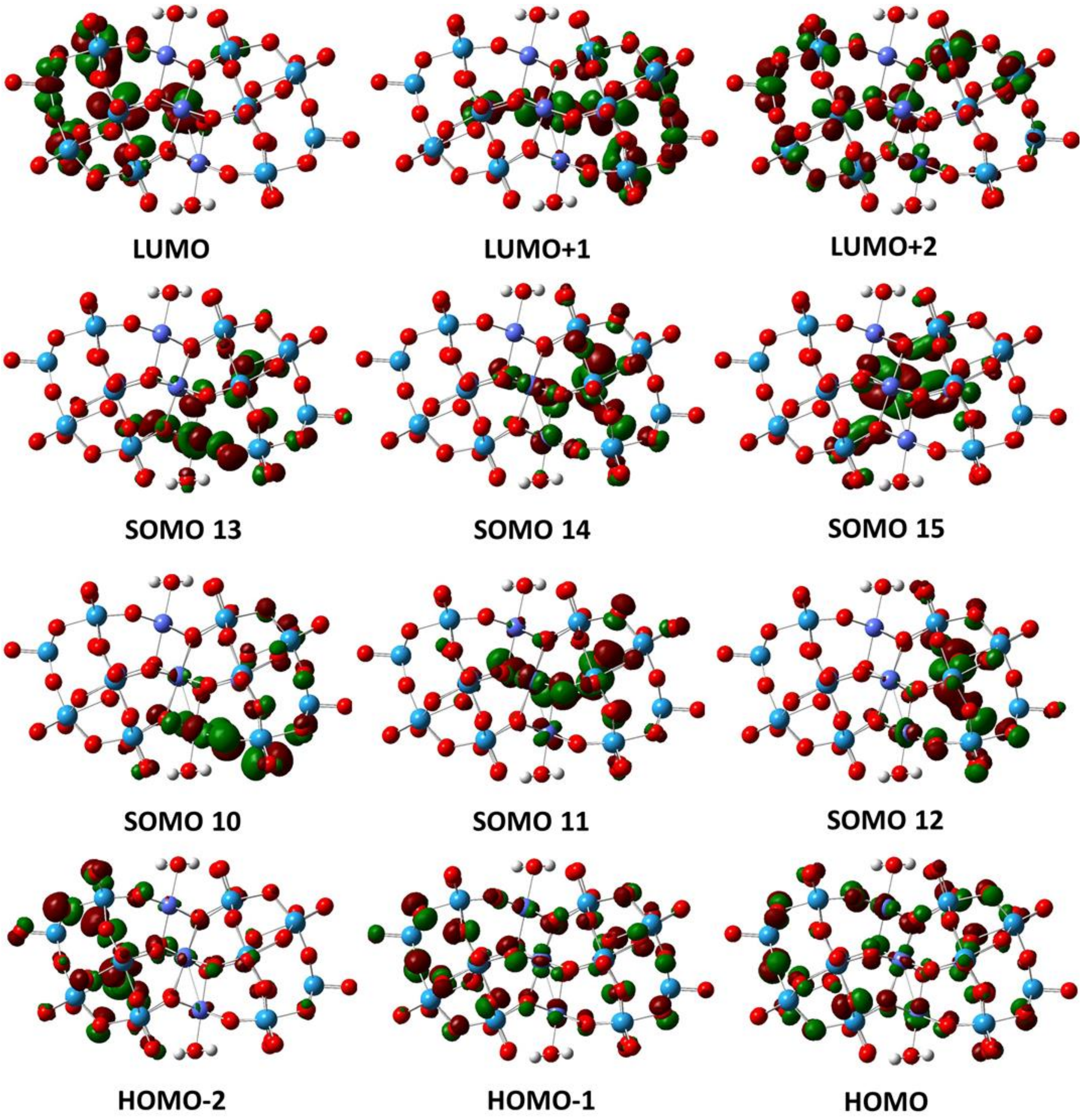

**Figure S2.** Frontier orbitals along with some important SOMOs of Co-WCo$_3$ POM. ($E_{HOMO}$ = -6.50 eV, $E_{LUMO}$ = -2.28 eV, ΔE = 4.22 eV, $E_{SOMO15}$ = -3.83 eV, $\Delta E_1$ = 1.55 eV, $E_{SOMO14}$= -5.76 eV, $\Delta E_2$= 3.48 eV where $\Delta E = E_{LUMO}-E_{HOMO}$, $\Delta E_1= E_{LUMO}-E_{SOMO15,}$ $\Delta E_2= E_{LUMO}-E_{SOMO14}$)

From the DFT study comparison of P-Co$_4$ and Co-WCo$_3$ POM, the band gap of P-Co$_4$ is 0.54 eV more than Co-WCo$_3$ POM, with their LUMO having almost similar energies. In the case of Co-WCo$_3$ POM, the SOMO-15 (highest energy electron present) is higher energy with $\Delta E_1$ only 1.55 eV (compared to $\Delta E_1$=4.19 eV in P-Co$_4$ POM) (Figure S1) partially due to the presence of tungsten at the sandwich position. Almost all SOMOs of Co-WCo$_3$ POM are high energetic than the highest energetic electron (SOMO-12) of P-Co$_4$ POM. During water oxidation, a change in spin state (high spin to low spin) of cobalt would make the SOMOs empty, which gives better feasibility for electron acceptance in the case of P-Co$_4$ compared to Co-WCo$_3$ POM, thus rendering the lower OER kinetics of Co-WCo$_3$. Also, SOMO-15 (highest energy electron) of Co-WCo$_3$ POM shows the contribution from the heteroatom Co also (overlapping of orbitals between Co heteroatom and Co in the sandwich position). In contrast, the SOMO-12 (highest energy electron) of P-Co$_4$

POM shows no such overlap between the heteroatom P and Co in the sandwich position. This heteroatom difference might also influence the activity at the external Co (in sandwich position) atom in these sandwich POMs.

## Characterization of $Na_{12}$[Co-$WCo_3$] and [PVIM][Co-$WCo_3$]

Compounds $Na_{12}$[Co-$WCo_3$] and [PVIM][Co-$WCo_3$] were characterized using electrospray ionization mass spectrometry (ESI-MS), single crystal X-ray spectroscopy (SC-XRD), Fourier transform infrared (FT-IR), and UV-visible spectroscopy. The FT-IR spectra of $Na_{12}$[Co-$WCo_3$] polyoxometalates show the characteristics peaks in the region 750-1000 $cm^{-1}$ (Figure S3) while [PVIM][Co-$WCo_3$] shows the characteristics peaks of C-N bond along with peaks of Co-$WCo_3$ POM in the region of 750-1000 $cm^{-1}$ (Figure S4). ESI-mass spectrum of Co-$WCo_3$ POM in Figure S5 shows the m/z value of 2461.79 for z equal to -2, 1628.53 for z equal to -3 and 1221.63 for z equal to -4 (Table S2). The framework structure was further confirmed by SC-XRD (**CCDC 1558372**) (Figure S6). The UV-visible spectra show a slight shift in maxima when Co-$WCo_3$ POM is heterogenized with PVIM (figure S7), and it shows broad charge transfer spectra in UV-visible region. The complexes of Co-$WCo_3$ POM with Cs and $C_{25}H_{54}N$ have been synthesized and characterized using FT-IR spectroscopy, and it shows the characteristics peaks of Co-$WCo_3$ POM in the region of 750-1000 $cm^{-1}$ (Figure S9).

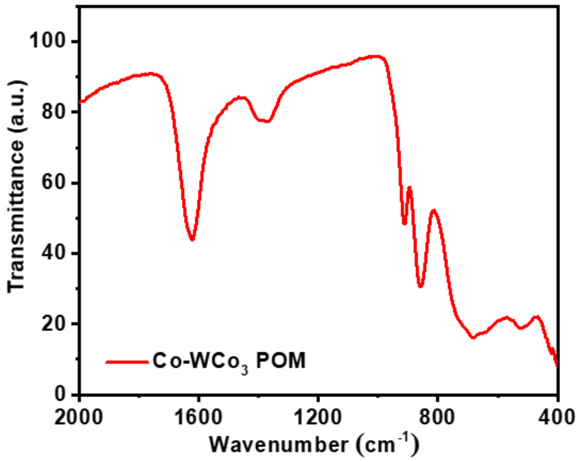

**Figure S3.** FT-IR spectra of $Na_{12}$[Co-$WCo_3$].

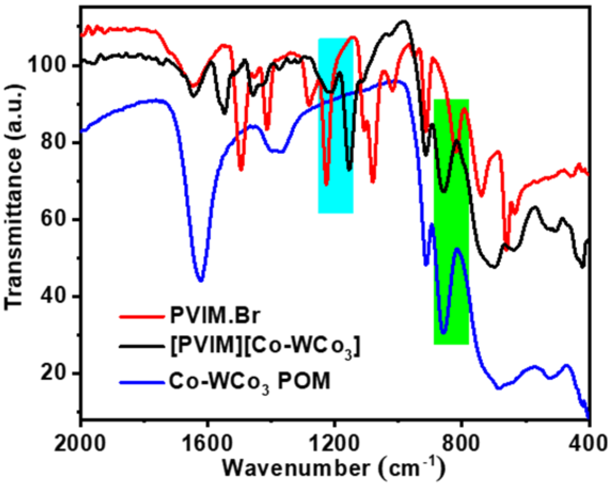

**Figure S4.** FT-IR spectra of [PVIM][Co-$WCo_3$].

## ESI mass spectrum and peak assignments for Na$_{12}$[Co-WCo$_3$]

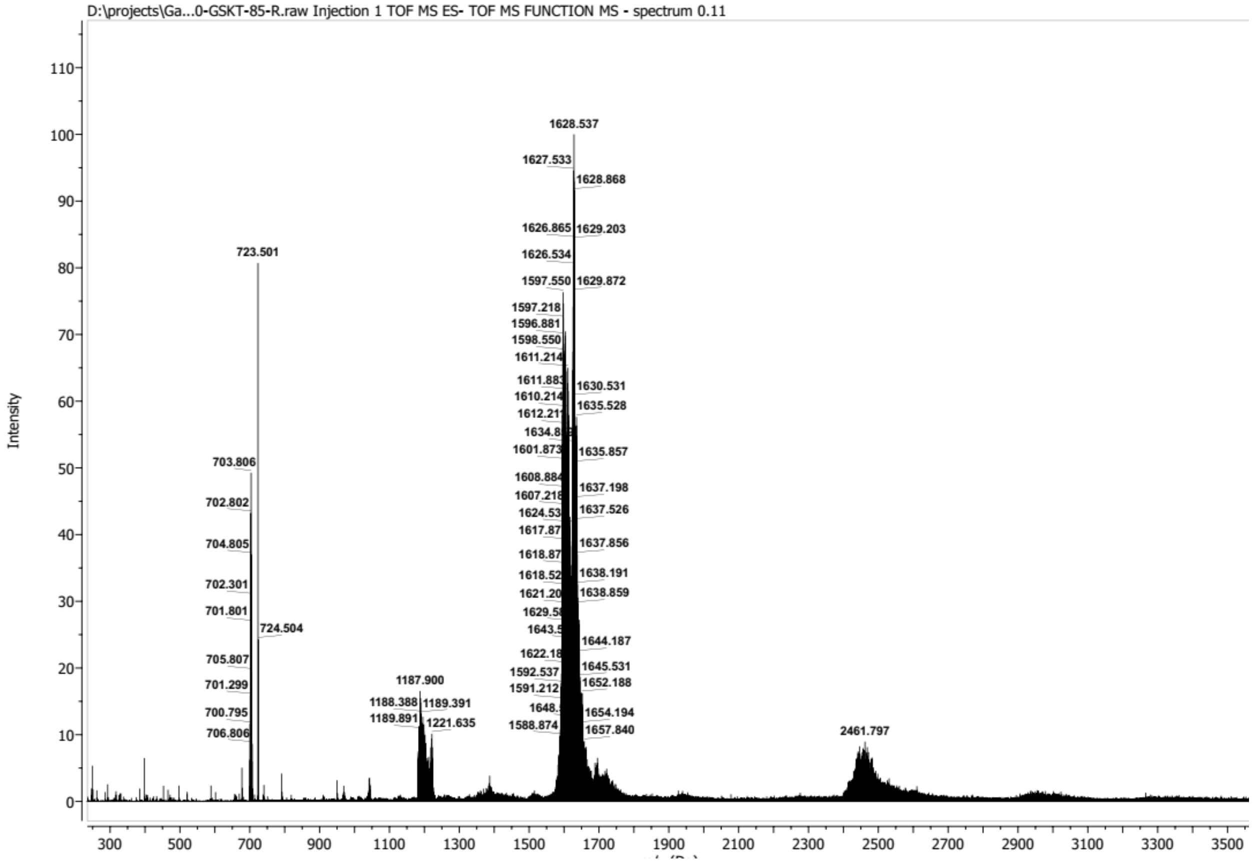

**Figure S5.** ESI mass spectrum (negative mode) of the aqueous solution of Na$_{12}$[Co-WCo$_3$].

**Table S2.** Assignment of m/z peaks in the ESI-MS spectra of Na$_{12}$[Co-WCo$_3$].

| Fragment | Mol. Wt. | z | m/z (cal.) | m/z (obs.) |
|---|---|---|---|---|
| $\{[WCo_3(CoW_9O_{34})_2]+9H\}^{3-}$ | 4884.36 | -3 | 1628.12 | 1628.53 |
| $\{[WCo_3(CoW_9O_{34})_2]+8H\}^{4-}$ | 4883.36 | -4 | 1220.84 | 1221.63 |
| $\{[WCo_3(CoW_9O_{34})_2]+9H+K\}^{2-}$ | 4923.34 | -2 | 2461.67 | 2461.79 |

## Single crystal X-ray analysis of $Na_{12}$[Co-$WCo_3$]

The molecular structure of $Na_{12}$[Co-$WCo_3$] was analyzed by single crystal X-ray diffraction (SC-XRD) analysis. The crystal data of Co-$WCo_3$ was matched with our previously reported data (CCDC no. 1558372). As observed from the molecular structure, the $WCo_3$ core of Co-$WCo_3$ was sandwiched by two $[CoW_9O_{34}]^{12-}$ (Co as heteroatom) units.

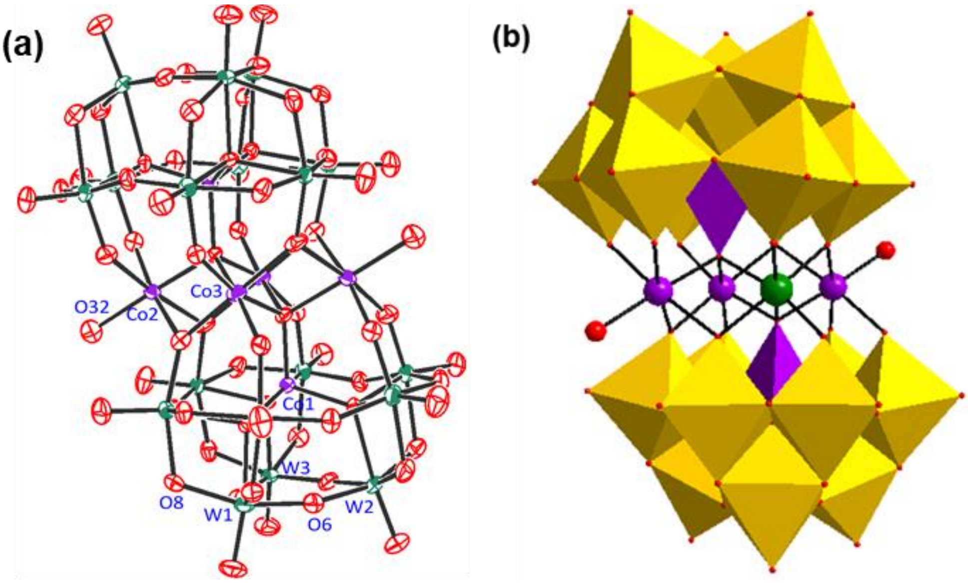

**Figure S6.** (a) ORTEP drawing (with 60% ellipsoid probability) and (b) combined polyhedral/ball-and-stick representation of the single-crystal X-ray structure of polyoxometalate anion $[WCo_3(H_2O)_2(CoW_9O_{34})_2]^{12-}$ [Co-$WCo_3$] (W = green; O = red; Co = purple; $WO_6$ = golden yellow octahedra; $CoO_4$ = purple tetrahedra); counter ions and hydrogen atoms of water are omitted for clarity.

### UV-vis. spectroscopy of $Na_{12}$[Co-$WCo_3$], [PVIM][Co-$WCo_3$] and [PVIM][P-$Co_4$]

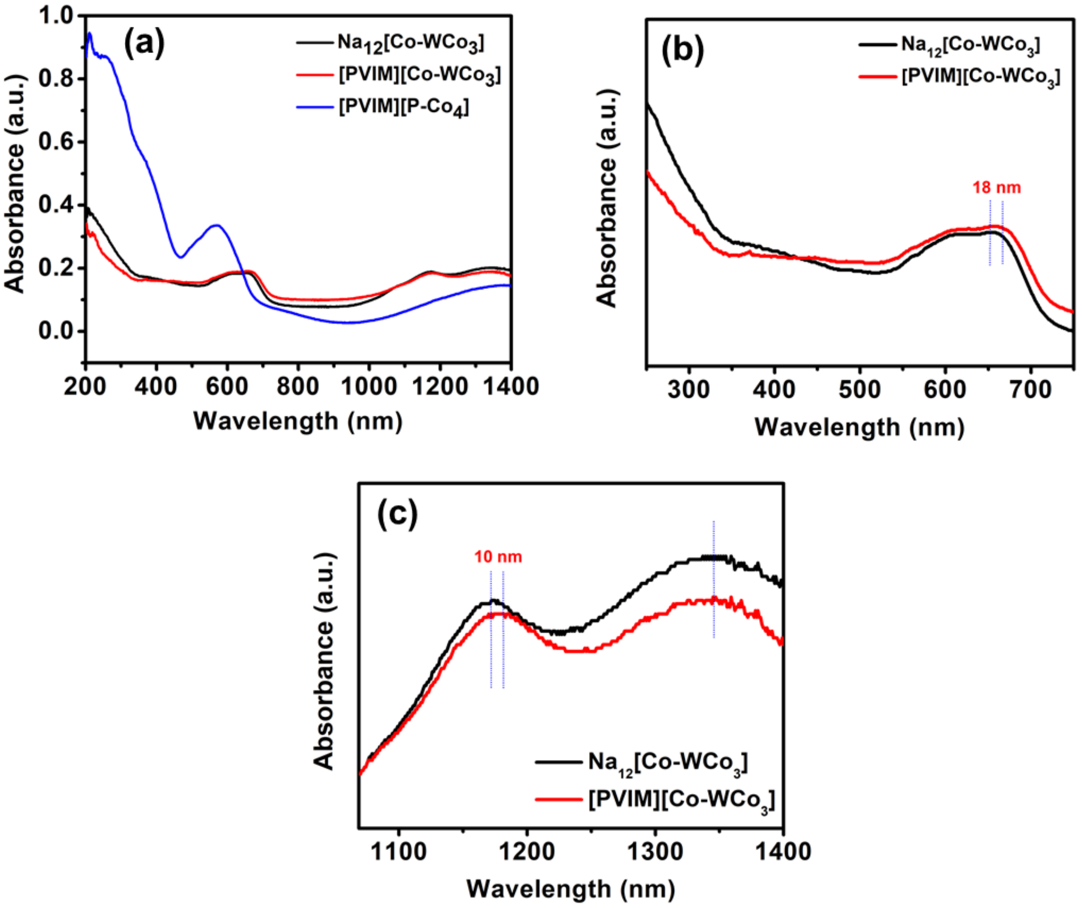

**Figure S7.** Solid-state UV-vis. spectra of (a) $Na_{12}$[Co-$WCo_3$], [PVIM][Co-$WCo_3$] and [PVIM][P-$Co_4$]; (b) and (c) Zoom in solid-state UV-vis. spectra of $Na_{12}$[Co-$WCo_3$], [PVIM][Co-$WCo_3$].

### TGA of $Na_{12}$[Co-$WCo_3$], [PVIM]Br and [PVIM][Co-$WCo_3$]

The thermal stability as well as the composition of [PVIM][Co-$WCo_3$] was determined by thermogravimetric analysis (TGA). The TGA traces of $Na_{12}$[Co-$WCo_3$], [PVIM]Br and [PVIM][Co-$WCo_3$] was performed from 25°C to 800 °C with a heating rate of 10 °C $min^{-1}$. The TGA curve of $Na_{12}$[Co-$WCo_3$] shows excellent thermal stability even up to 800 °C (Figure S6). Initially, the hydrated water molecules were evaporated from $Na_{12}$[Co-$WCo_3$] in the temperature range of 25 °C to 200 °C with a weight loss of 4.5%. The number of hydrated water molecules was calculated to be 12 per $Na_{12}$[Co-$WCo_3$] molecule. However, in between 200-670 °C there was only 3.9% weight loss, suggests the minor thermal decomposition of $Na_{12}$[Co-$WCo_3$]. Whereas, [PVIM]Br shows thermal decomposition of ~97% in between 250-500 °C, suggesting the comparative poor thermal stability. The TGA curve of [PVIM][Co-$WCo_3$] shows weight loss of ~35.2% up to 800 °C. The thermogravimetric analysis (TGA) shows the composition of Co-$WCo_3$

in [PVIM][Co-WCo3] was ~72 wt.% and was matching with the composition used during the synthesis of composite.

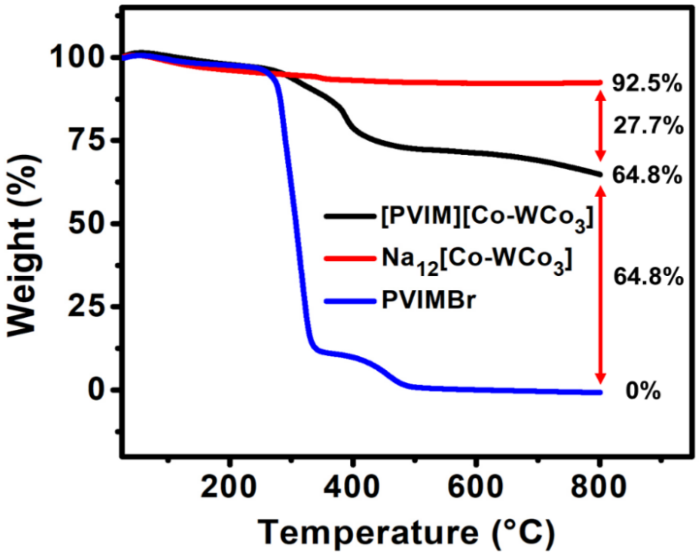

**Figure S8.** TGA curve of $Na_{12}$[Co-$WCo_3$], [PVIM][Co-$WCo_3$] and [PVIM]Br.

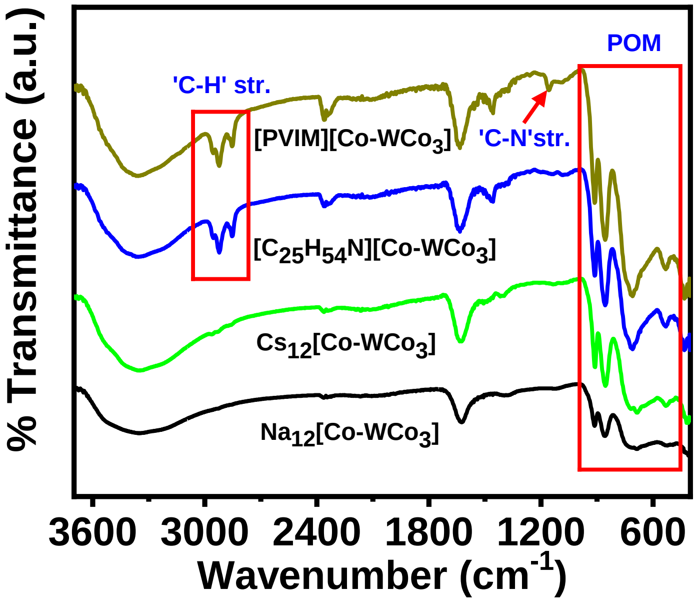

**Figure S9.** FT-IR spectra of $Na_{12}$[Co-$WCo_3$], $Cs_{12}$[Co-$WCo_3$], [$C_{25}H_{54}N$]$_{12}$[Co-$WCo_3$] and [PVIM][Co-$WCo_3$].

**Characterization of ZIF-8 and [Co-WCo3]@ZIF-8**

[Co-$WCo_3$]@ZIF-8 was characterised using FT-IR, Raman, PXRD and UV-visible spectroscopy (Figures S10-S13). FT-IR spectra showing the characteristics peaks of ZIF-8 and Co-$WCo_3$ polyoxometalate in the composite material (Figure S10). UV-visible spectra of Co-$WCo_3$ showing the charge transfer from oxygen to tungsten in the UV region as well as d-d transition in the visible region. The composite Co-$WCo_3$@ZIF-8 shows a broad spectrum in the UV-visible region indicating both polyoxometalate and ZIF-8 are present in the composite materials (Figure S11). PXRD of Co-WCo$_3$@ZIF-8 shows the crystalline nature of the composite containing characteristic peaks of ZIF-8 as well as Co-WCo$_3$ polyoxometalate (Figure S12). Raman Spectra of Co-WCo$_3$@ZIF-8 showing characteristics peaks of ZIF-8 in the composite as well the characteristics peak of Co-WCo$_3$ polyoxometalates at 951 cm$^{-1}$ (Figure S13).

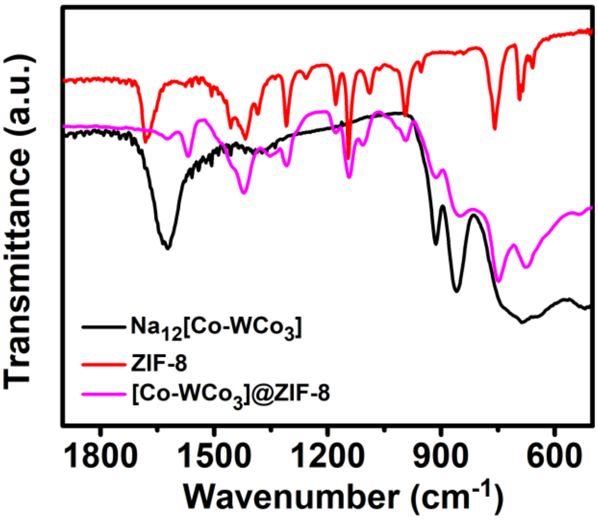

**Figure S10.** FT-IR spectra of ZIF-8, Na$_{12}$[Co-WCo$_3$] and [Co-WCo$_3$]@ZIF-8.

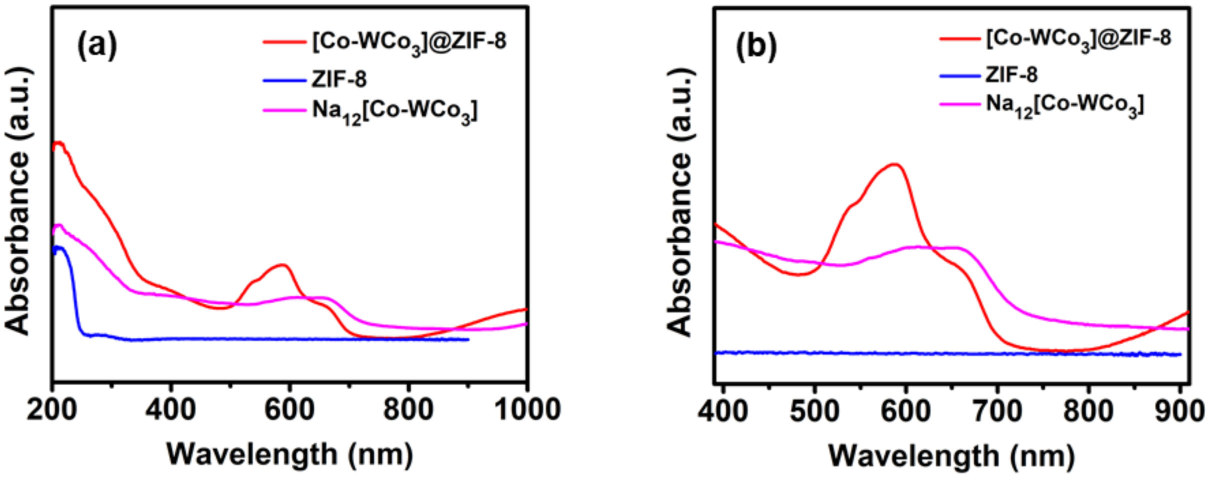

**Figure S11.** UV-vis spectra of ZIF-8, Na$_{12}$[Co-WCo$_3$] and [Co-WCo$_3$]@ZIF-8.

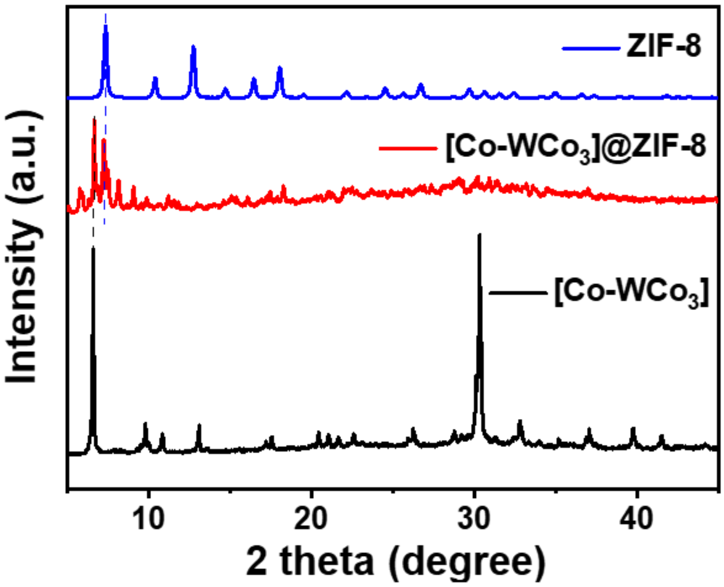

**Figure S12.** Powder XRD of ZIF-8, $Na_{12}$[Co-$WCo_3$] and [Co-$WCo_3$]@ZIF-8.

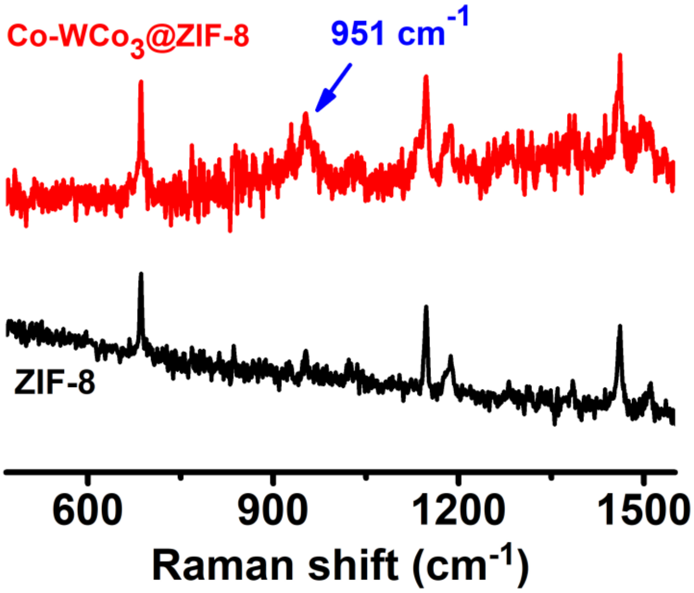

**Figure S13.** Raman spectroscopy of ZIF-8 and [Co-$WCo_3$]@ZIF-8.

### Characterization of $Na_{12}$[V-$Co_4$] and [PVIM][V-$Co_4$]

$Na_{12}$[V-$Co_4$] was prepared according to the previously reported literature,[5] and the FT-IR spectra show the characteristic peaks of POM in the region of 750-1000 cm$^{-1}$ (Figure S14). The SC-XRD structure of V-$Co_4$ depicted in Figure S15 revealed that is isostructural with Co-$WCo_3$ POM. $^{51}$V NMR spectrum of $Na_{10}$[V-$Co_4$] in $H_2O$ shows two peaks (-506.85 and -332.17 ppm, Figure S16). Though the peak at -506 ppm is reported in the literature, the correct value is difficult to assign due to less stability of V-$Co_4$ POM in solution. The time-dependent $^{51}$V NMR study in Figure S17 of the PVIM composite shows that the V-$Co_4$ POM is less stable in aqueous solution. A new peak at

~550 ppm appeared after 2 h in $^{51}V$ NMR spectra of [PVIM][V-$Co_4$] in 1M KOH, which depicts the less stability of the composite.

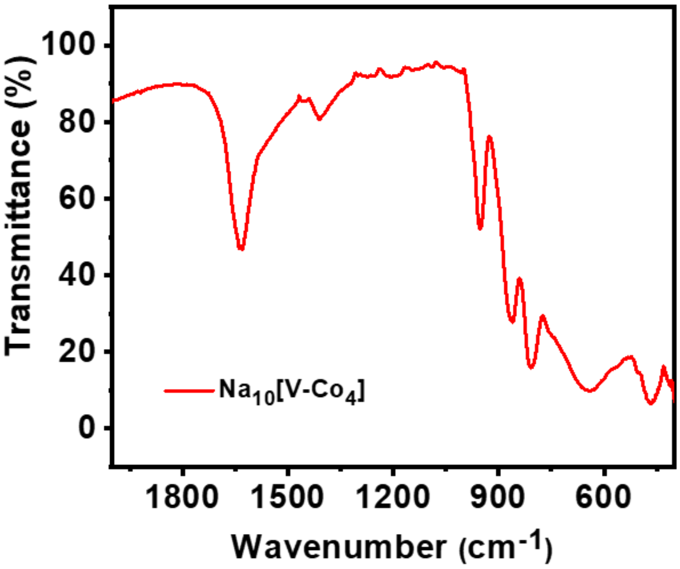

**Figure S14.** FT-IR spectrum of $Na_{10}$[V-$Co_4$].

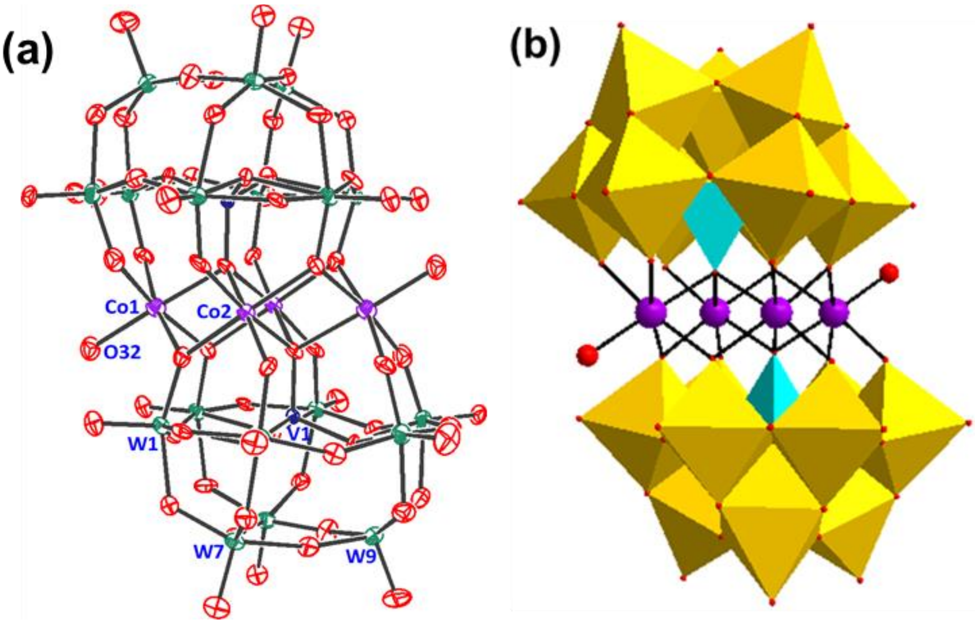

**Figure S15.** (a) ORTEP drawing (with 60% ellipsoid probability) and (b) combined polyhedral/ball-and-stick representation of the single-crystal X-ray structure of $Na_{10}[Co_4(H_2O)_2(VW_9O_{34})_2]$ (V-$Co_4$) (**CCDC number 2241107;** W, green; O, red; Co, purple; V, turquoise; $WO_6$ = golden yellow octahedra; $VO_4$ = turquoise tetrahedra)). Counter cations and hydrogen atoms are omitted for clarity.

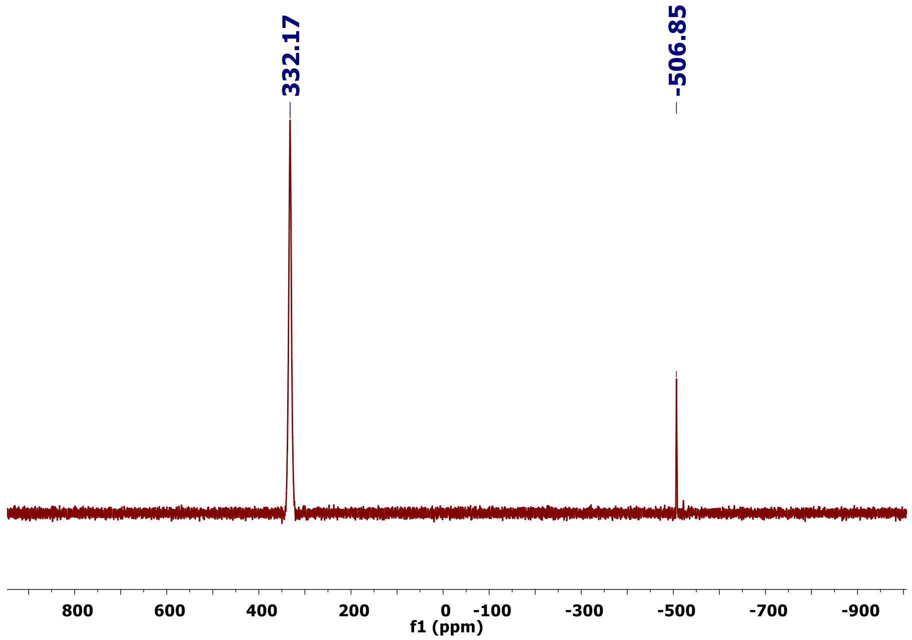

**Figure S16.** $^{51}$V NMR spectra of $Na_{10}[V\text{-}Co_4]$ in $H_2O$.

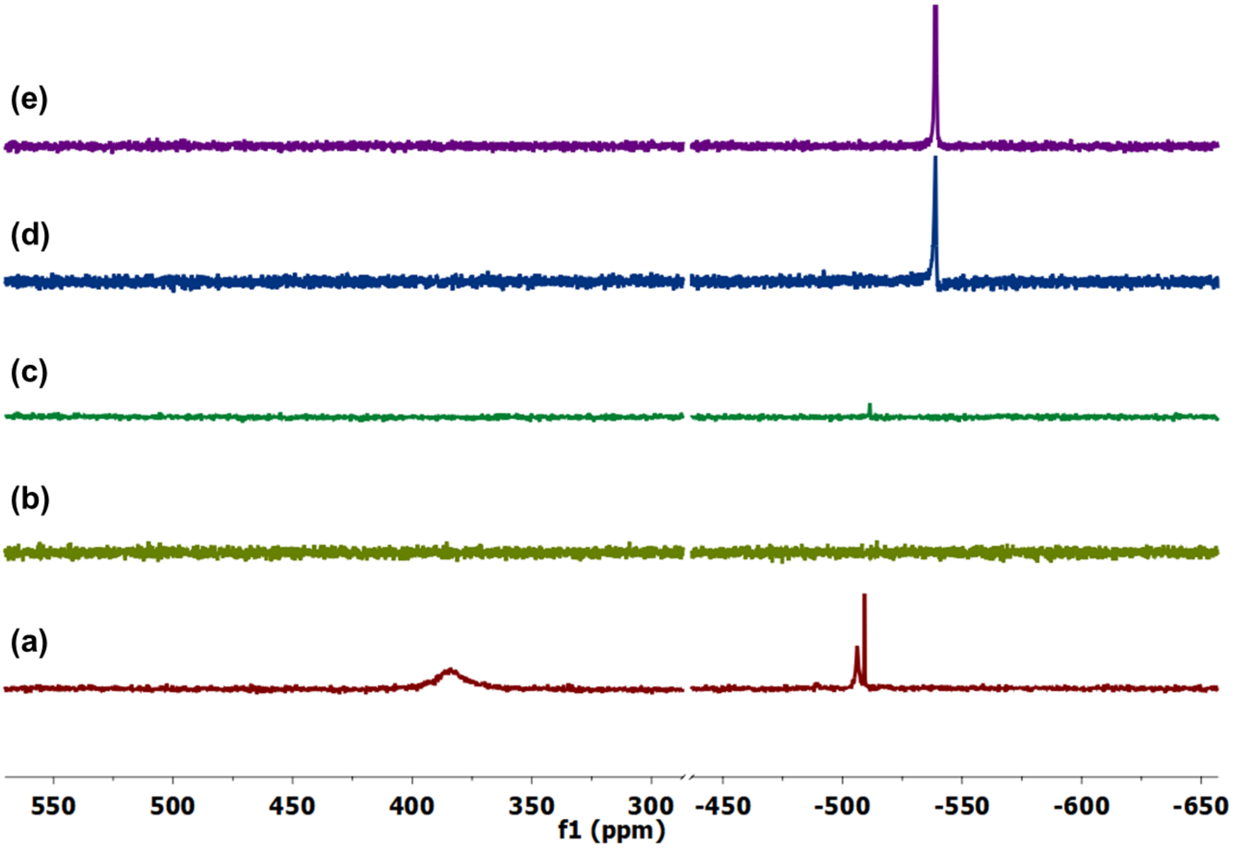

**Figure S17.** $^{51}$V NMR spectra of (a) $Q_{10}[V\text{-}Co_4]$ ($Q = C_{25}H_{54}N$) in $CH_3CN$ (b) [PVIM][V-$Co_4$] in NaPi buffer (pH 7) after 2 h (c) [PVIM][V-$Co_4$] in NaPi buffer (pH 7) after 4 days (d) [PVIM][V-$Co_4$] in 1M KOH after 2 h and (e) [PVIM][V-$Co_4$] in 1M KOH after 24 h.

### [PVIM][Co-WCo$_3$] catalyzed water oxidation

### Alternative cyclic voltammetry and chronopotentiometric study

The activity and efficiency of water oxidation catalysts, in terms of overpotential, can be compared by alternative cyclic voltammetry and chronopotentiometric study at a fixed current density of 10 mAcm$^{-2}$ (used for benchmark studies for OER). Therefore, electrocatalytic water oxidation of [PVIM][Co-WCo$_3$] was investigated by an alternative cyclic voltammetry and chronopotentiometric study at a fixed current density of 10 mAcm$^{-2}$. Initially, the potential required to reach 10 mAcm$^{-2}$ was 1.66 V (*vs*. RHE) and then remained constant at 1.51 V (*vs*. RHE) till the end of the measurement (30 h) (Figure 2d). Therefore, the overpotential required to reach the benchmark current density (10 mA cm$^{-2}$) was 0.28 V, which is comparable to noble-metal based catalysts. Again, the constancy of potential (1.51 V *vs*. RHE) up to 30 h, shows the long-term stability of the catalyst.

### Cyclic voltammograms of [PVIM][Co-WCo$_3$] composite

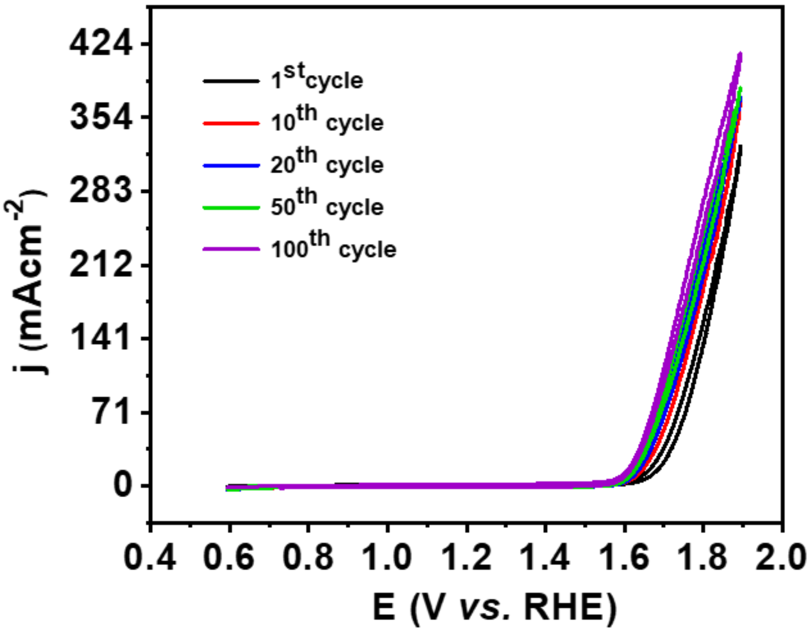

Figure S18. Cyclic voltammogram of [PVIM][Co-WCo$_3$] up to 100th cycle in 1 M KOH solution at a scan rate of 50 mV/s.

## Chronroamperometric pulse measurement

To determine the onset potential of OER (in pH 14), chronoamperometric measurements were performed (from 0.05 V to 0.75 V) with a potential step of 50 mV after every 2 min. and the corresponding $J_k$ were recorded. The sudden jump in current density in the plot of absolute $J_k$ *vs*. applied potential indicates the start of OER at 1.55 V (*vs*. RHE).

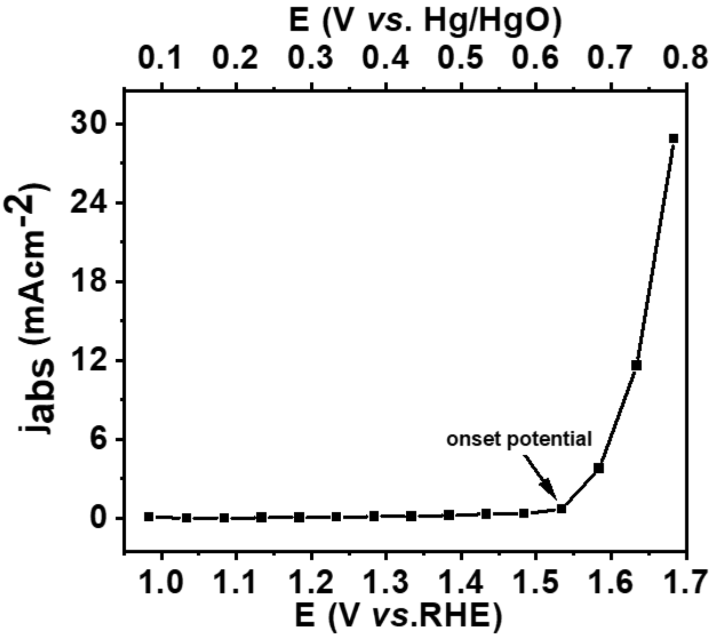

**Figure S19.** Chronroamperometric pulse measurement for OER in 1M KOH electrolyte with a potential step of 50 mV after every 2 min.

## Tafel plot

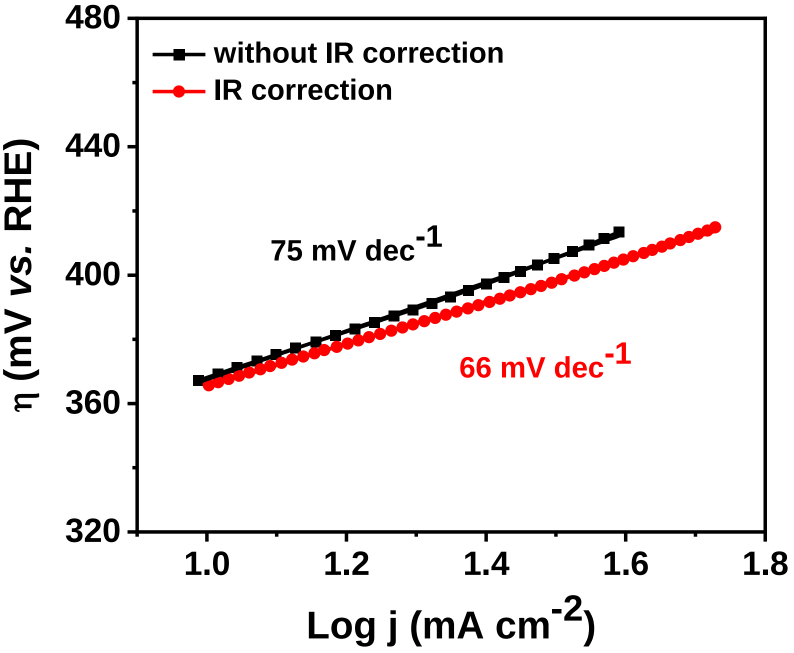

**Figure S20.** Tafel plot of [PVIM][Co-WCo3] (extracted from CV).

## Electrochemical Impedance Spectroscopy (EIS)

Electrochemical impedance studies were performed for [PVIM][Co-$WCo_3$] in the frequency range from 0.1 Hz to 100 kHz, and the resulting Nyquist plot was plotted (Figure S21). The differential activity of [PVIM][Co-$WCo_3$] composite in two different solutions of pH 8 (sodium phosphate buffer) and pH 14 (1M KOH) could be due to the kinetics of interfacial charge transfer process. As evident from Figure S21, lower charge transfer resistance at pH 14 compared to pH 8 indicates faster kinetics and facilitated electron transfer at the catalyst surface in alkaline medium.

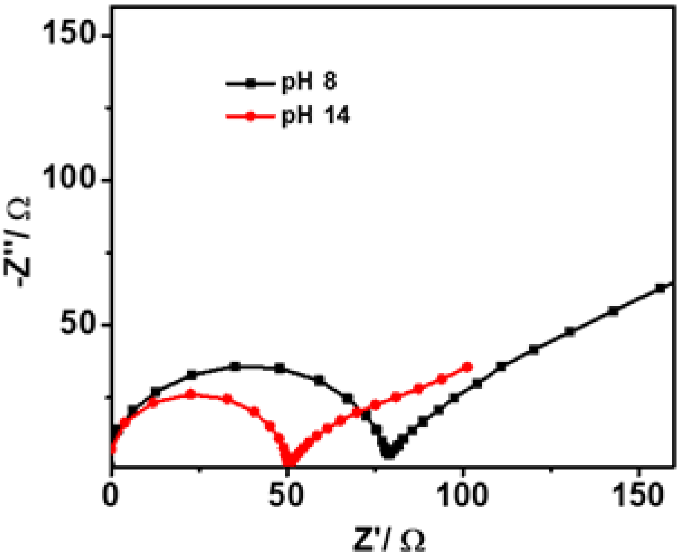

**Figure S21.** Impedance spectra of [PVIM][Co-$WCo_3$] composite in 1 M KOH and sodium phosphate buffer (pH 8) solution. CE: Pt mesh; RE: Hg/HgO/1M KOH.

## Electrochemical surface area (ECSA) measurement

The electrocatalytic activity is directly related to the electrochemical surface area (ECSA) of the catalyst, which shows the available active sites of the catalyst for substrates. ECSA of [PVIM][Co-$WCo_3$] in 1M KOH solution was found to be 2.38 $cm^2$ (ECSA of [PVIM][P-$Co_4$] was 2.10 $cm^2$), which supports the superior activity of the catalyst. However, in sodium phosphate buffer solution (pH 8), the ECSA was found to be 0.29 $cm^2$ (ECSA of [PVIM][P-$Co_4$] was 0.28 $cm^2$), which shows the less active sites and is reflected in cyclic voltammetry analysis.

The electrochemical surface area of the catalyst was determined by computing the double-layer pseudo-capacitance ($C_{dl}$) of the composite in 1M KOH solution.

| **Determination of electrochemical surface area (ECSA) at pH 14.** | | | |
|---|---|---|---|
| **Catalyst** | **$C_{dl}$ (µF) at 0.88 V vs. RHE** | **ECSA ($cm^2$)** | **Roughness factor** |
| **[PVIM][Co-WCo$_3$]** | 95.445 | 2.38612 | 33.75 |

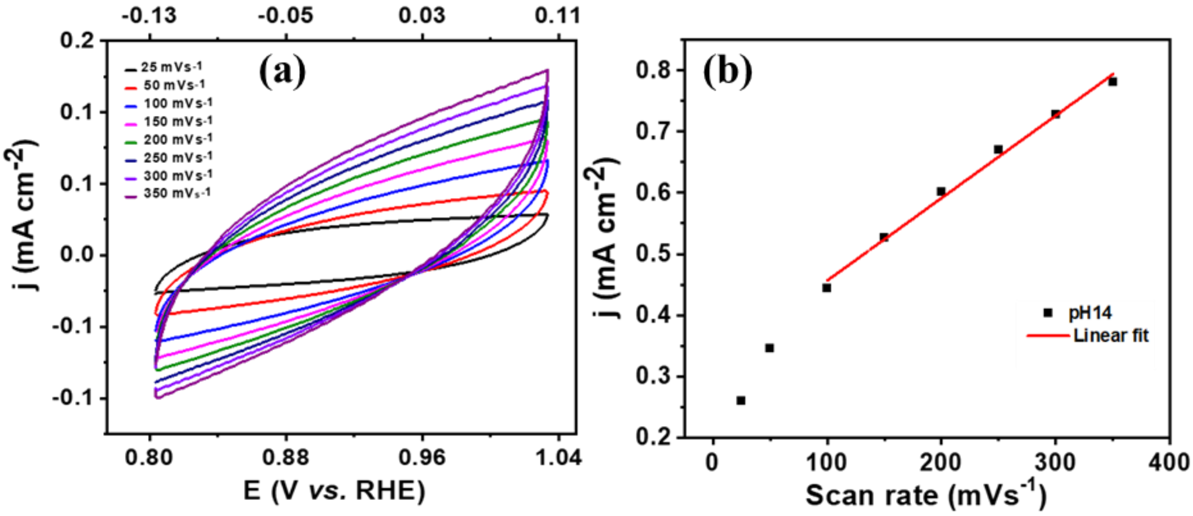

**Figure S22. (a)** Cyclic voltammograms for [PVIM][Co-WCo$_3$] composite at varying scan rates (25 mV $s^{-1}$ to 350 mV $s^{-1}$) in the non-faradic potential region and (b) corresponding average current density versus scan rate at pH 14. (CE: Pt mesh, RE: Hg/HgO/1M KOH).

| **Catalyst** | **$C_{dl}$ (µF) at 0.64 V vs. RHE** | **ECSA ($cm^2$) pH 8** | **Roughness factor** |
|---|---|---|---|
| [PVIM][Co-WCo$_3$] | 11.8069 | 0.295 | 4.15 |

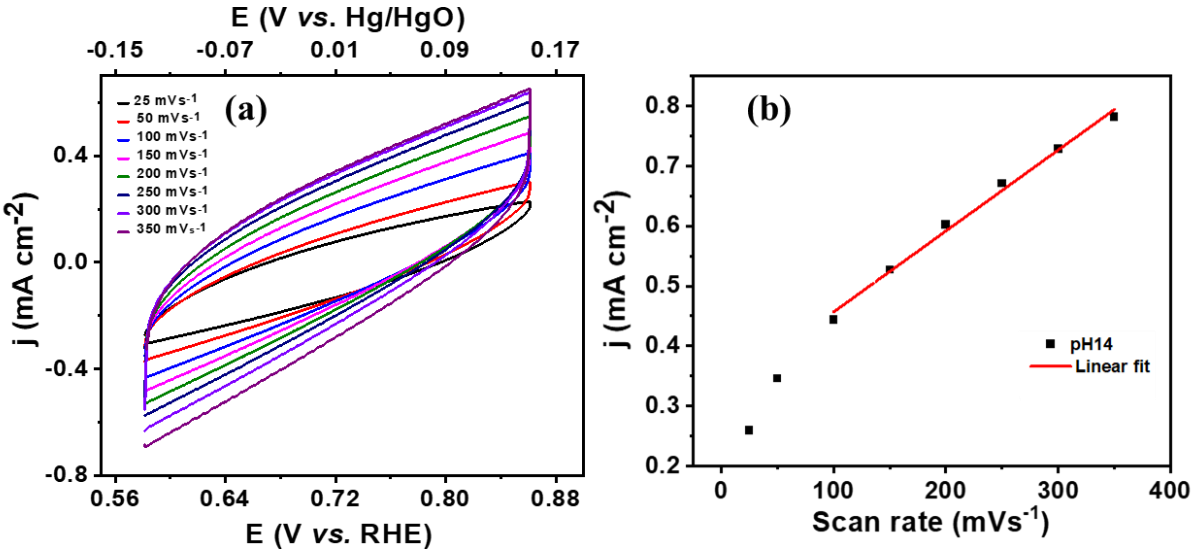

**Figure S23. (a)** Cyclic voltammograms for [PVIM][Co-WCo$_3$] composite at varying scan rates (25 mV s$^{-1}$ to 350 mV s$^{-1}$) in the non-faradic potential region in sodium phosphate buffer (0.1M) and (b) corresponding average current density versus scan rate at pH 8 solution (CE: Pt mesh, RE: Hg/HgO/1M KOH).

## Analysis of evolved oxygen using gas chromatography (GC)

The gas chromatographic (GC) analysis was performed for the quantitative estimation of the evolved oxygen gas during the course of OER. Before quantification, the known oxygen and nitrogen gas samples (100 µL of each in two separate experiments) were injected in the GC by using Hamilton gas tight syringe to know the retention time of the respective gases. For quantitative estimation, the experimental set-up was comprised of three-electrode system connected to the potentiostat, and the electrodes were placed in an air-tight electrochemical cell filled with deaerated 1 M KOH solution. The catalyst (0.1 mg) was drop-coated over graphite paper strip, which acts as working electrode along with Pt mesh counter electrode referenced against Ag/AgCl/3M KCl. The air-tight electrochemical cell and the electrolyte solution were fully deaerated by purging N$_2$ gas bubbled through the KOH solution for 30 min. The N$_2$ gas was bubbled through the electrolyte solution for 30 min. to fully deaerated the air-tight electrochemical cell and the dissolved O$_2$ of the electrolyte solution. Before starting the experiment, the open circuit potential (OCP) was monitored for 15 min, and then the gas sample was analyzed by GC. The chronoamperometric experiment was subsequently performed at a potential of 1.75 V (*vs.* RHE), and the gas sample (100 µL) from the reaction vessel head-space was injected in GC to analyze the amount of evolved O$_2$. The separate Calibration experiment was performed by using exactly same procedure, replacing the reaction solution with water. The amount of evolved O$_2$ (in mmol) was calculated by taking the slope (m) and intercept (c) from the linear fitted calibration curve (Pearson r-value > 0.99). The turnover number (TON) of the catalyst was calculated as:

$$\mathbf{TON} = \frac{\textbf{Amount of evolved } \mathbf{O_2} \textbf{ (mmol)}}{\textbf{Amount of catalyst (mmol)}} = \mathbf{7393}$$

Whereas, the turnover frequency (TOF) was calculated as:

$$\mathbf{TOF} = \frac{\textbf{TON}}{\textbf{time}} = \frac{\textbf{7393}}{\textbf{1200 (sec)}} = \mathbf{6.16\ s^{-1}}$$

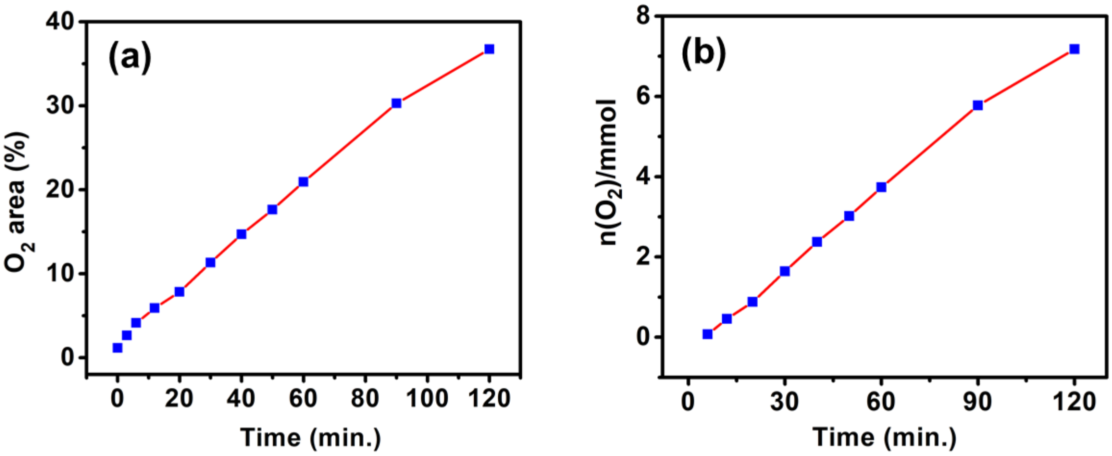

**Figure S24.** (a) Increase in the amount of oxygen in reaction vessel with time (the oxygen area% data extracted from GC analysis) and (b) kinetics of oxygen formation from water**.**

Faradaic efficiency Calculation.[6]

The faradaic efficiency of [PVIM][Co-WCo3] catalyst was calculated from the same experiment performed for quantitative estimation of the evolved oxygen. The amperometric experiment with an input potential of 1.71 V (*vs*. RHE) for 20 minutes reaching a current of 13.4 mA. The theoretical number of moles of oxygen evolved [$\eta_{O2}$ (theo.)] was calculated from Faraday's 2nd law of electrolysis, as follows-

$$\eta_{O_2}(\text{theo.}) = \frac{Q}{nF} = \frac{i\ x\ t}{nF}$$

$$= \frac{0.0134\ (A)\ x\ 1200\ (s)}{4\ x\ 96485.3\ s\ A\ \text{mol}^{-1}} = 4.16\ x\ 10^{-5}\ \text{mol}$$

Where $\eta_{O2}$ = number of moles of produced oxygen, Q = total charge passed during OER, n = number of electrons transferred during OER (4e), i = applied current (amperes), t = electrolysis time (second), and F = Faraday constant (96485.3 s A mol$^{-1}$).

The total number of moles oxygen produced after 20 minutes OER (as calculated from gas chromatographic analysis) is 3.69 x 10$^{-5}$ mol.

So, the faradaic efficiency

$$= \frac{\eta_{O_2}(\text{exp.})}{\eta_{O_2}(\text{theo.})} = \frac{3.69\ x\ 10^{-5}\ \text{mol}}{4.16\ x\ 10^{-5}\ \text{mol}} = 88.7\ \%$$

## Importance of PVIM toward activation and stabilization of Co-WCo3 for EWO

To understand the importance of PVIM toward the stabilization, activation and enhancement of EWO activity of Co-WCo3, control experiments were performed.

### Control experiment 1

In this experiment, the cyclic voltammetry of $Na_{12}$[Co-WCo3] and [PVIM][Co-WCo3] was performed in 1 M KOH solution.

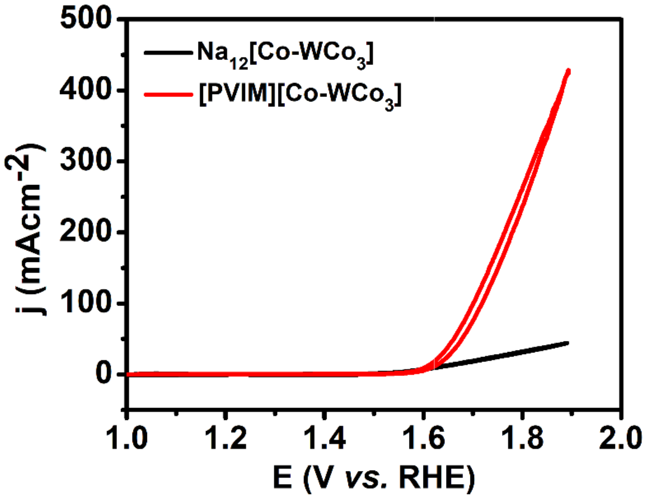

**Figure S25.** Cyclic voltammogram of 500 μM $Na_{12}$[Co-WCo3] dissolved in 1 M KOH solution (black line curve) and [PVIM][Co-WCo3] composite (coated on GC electrode) in 1 M KOH solution (red line curve).

The cyclic voltammetry of 500 μM $Na_{12}$[Co-WCo3] dissolved in 1M KOH (pH 14) shows the electrocatalytic water oxidation with a maximum current density of 44 mAcm$^{-2}$ at 1.89 V (*vs.* RHE), which started decreasing after 10 cycles. However, in the case of [PVIM][Co-WCo3], water oxidation starts at 1.6 V (*vs.* RHE) with a maximum current density of 428 mAcm$^{-2}$ at 1.89 V (*vs.* RHE). This experiment implies that in pH 14 the ionic polymer PVIM can activate Co-WCo3 towards electrocatalytic water oxidation.

### Control experiment 2

OER performance of $Cs_{12}$[Co-WCo3] and [$C_{25}H_{54}N$][Co-WCo3] *versus* [PVIM][Co-WCo3] in 1 M KOH solution.

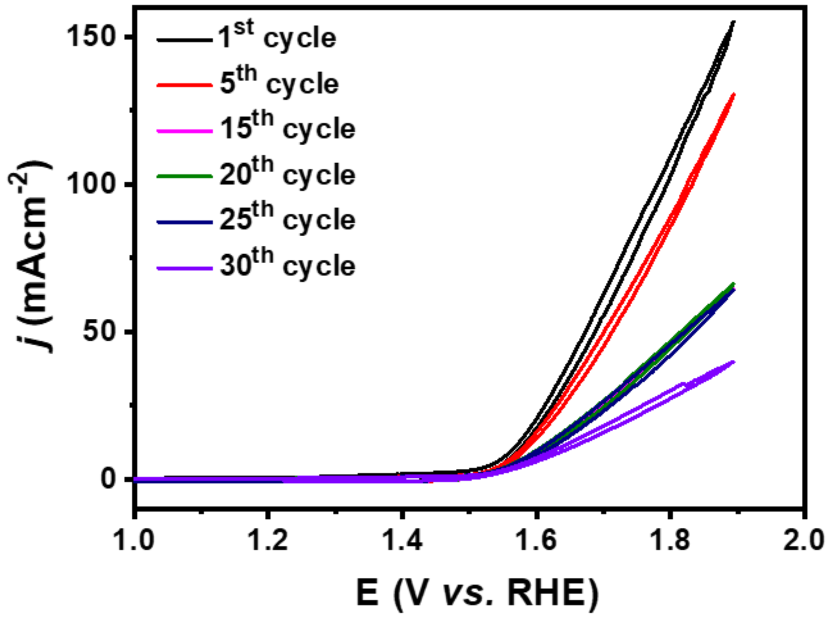

**Figure S26.** Cyclic voltammogram of $Cs_{12}[Co\text{-}WCo_3]$ (coated on glassy carbon electrode) in 1M KOH solution.

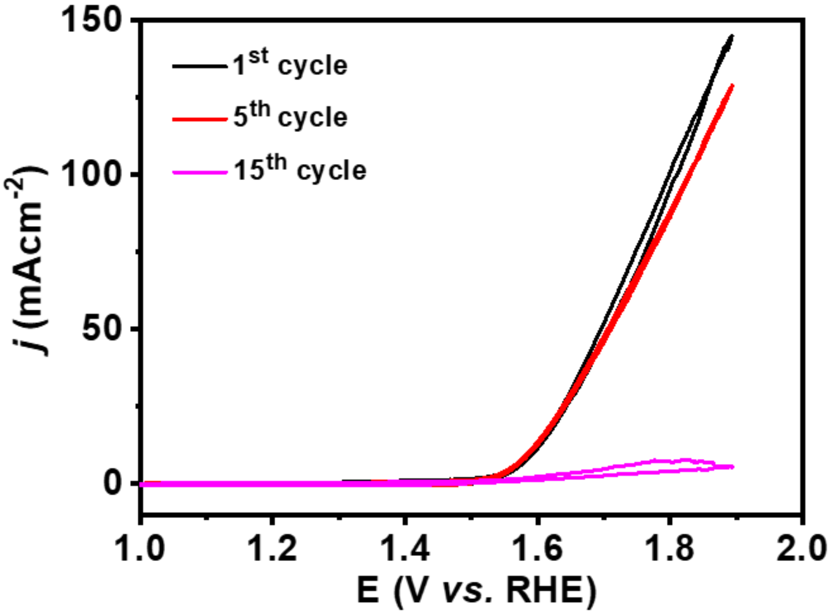

**Figure S27.** Cyclic voltammogram of $[C_{25}H_{54}N][Co\text{-}WCo_3]$ (coated on glassy carbon electrode) in 1M KOH solution.

## Co-WCo3@ZIF-8 catalyzed water oxidation

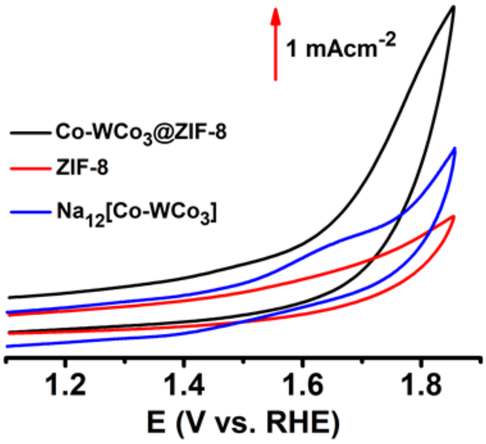

**Figure S28.** Cyclic voltammetry of ZIF-8 (drop-coated on the GC electrode), $Na_{12}[Co\text{-}WCo_3]$ (dissolved in 0.1 M $Na_2SO_4$ solution, pH 7) and $[Co\text{-}WCo_3]$@ZIF-8 (drop-coated on the GC electrode) in neutral media.

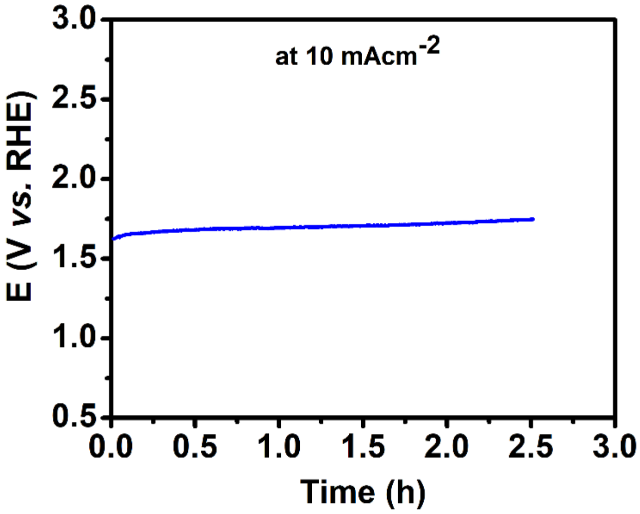

**Figure S29.** Chronopotentiometric curves (E-*t*) of $[Co\text{-}WCo_3]$@ZIF-8 at a fixed current density of 10 mA/cm$^2$ in 1M KOH. CE: Pt mesh; RE: Hg/HgO/1M KOH.

### Post-electrolysis characterization of [PVIM][Co-WCo$_3$] composite

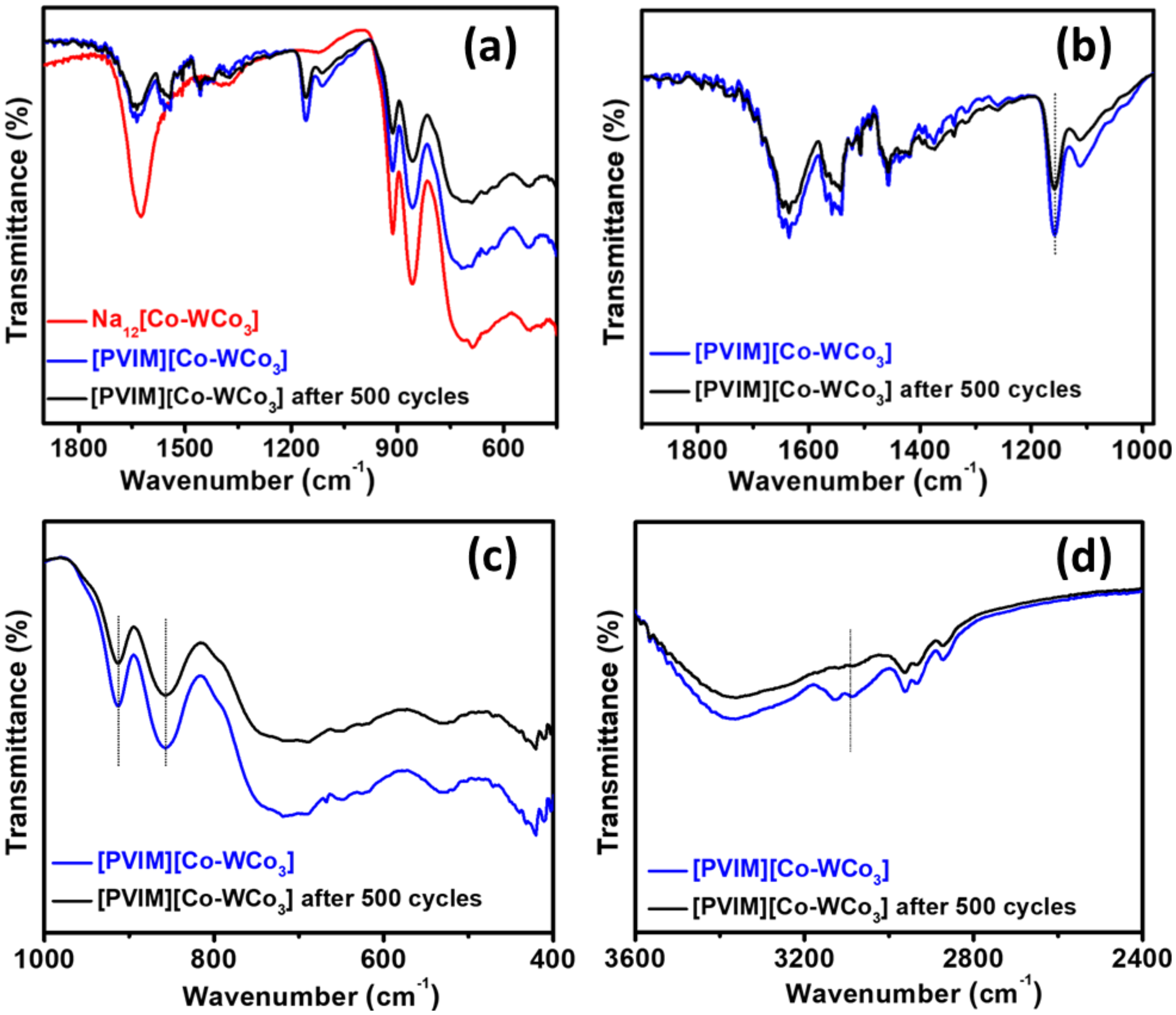

**Figure S30.** (a) FT-IR spectroscopy of $Na_{12}$[Co-WCo$_3$], [PVIM][Co-WCo$_3$] and [PVIM][Co-WCo$_3$] after 500 cycles of electrolysis; FT-IR spectrum of [PVIM][Co-WCo$_3$] before and after 500 cycles of electrolysis; (b) zoomed portion 1900-1000 cm$^{-1}$, (c) 1000-400 cm$^{-1}$and (c) 3600-2400 cm$^{-1}$.

To understand the stability of the catalyst, FT-IR and XP survey spectra before and after OER electrolysis were compared (Figure S30, S32). The FT-IR spectra shows no shifting in the characteristics peak of C-N bond at 1156 cm$^{-1}$ and POM peaks at 856 and 914 cm$^{-1}$ (Figure S30). The XP survey spectra before and after OER electrolysis shows similar patterns, and no impurity is observed (Figure S32). These post electrolysis experiments confirm that the catalyst is highly stable and the structure is not destructed during OER. Further, to check the catalyst stability in alkaline media, 0.5 mL 1M KOH solution was added to 0.1 g of [PVIM][Co-WCo$_3$]. After 1 day, the catalyst was dried and FT-IR was recorded. The FT-IR shows no change in the peaks further confirms the stability of the catalyst in alkaline media (Figure S31).

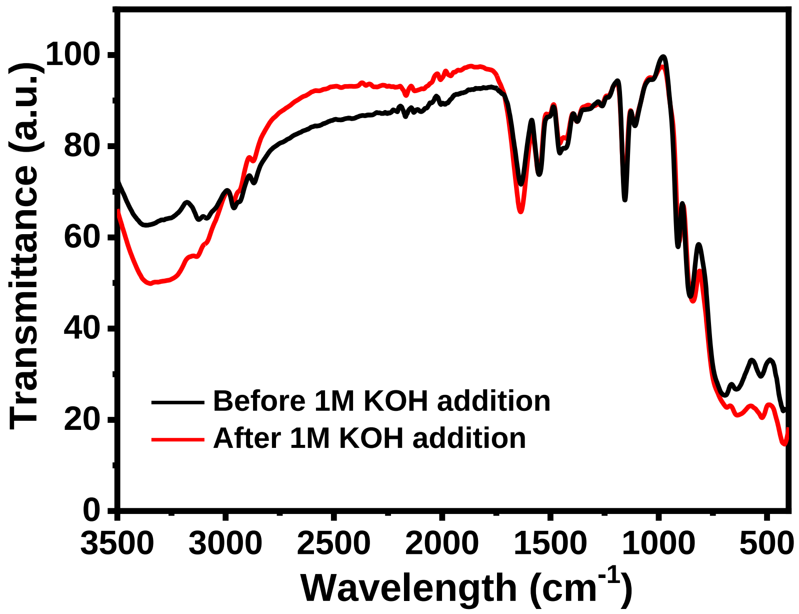

**Figure S31**. FT-IR spectra of [PVIM][Co-WCo3] before and after addition of 1M KOH (after one day).

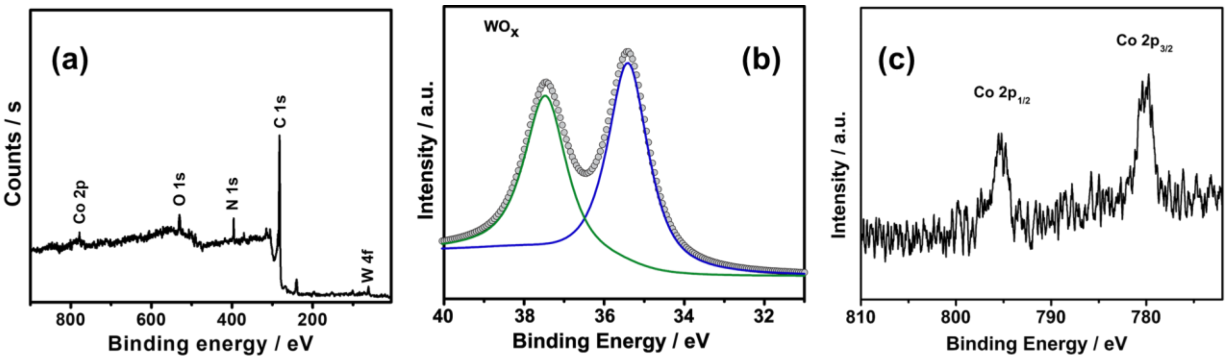

Post OER electrolysis

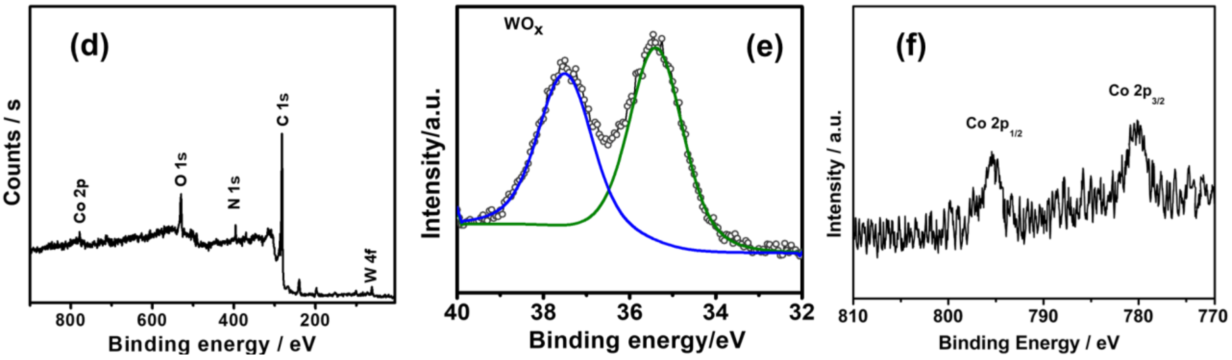

**Figure S32**. XP spectra of [PVIM][Co-WCo3] before OER electrolysis (a-c) and post OER electrolysis (d-f)

## Spectroelectrochemical study of water oxidation

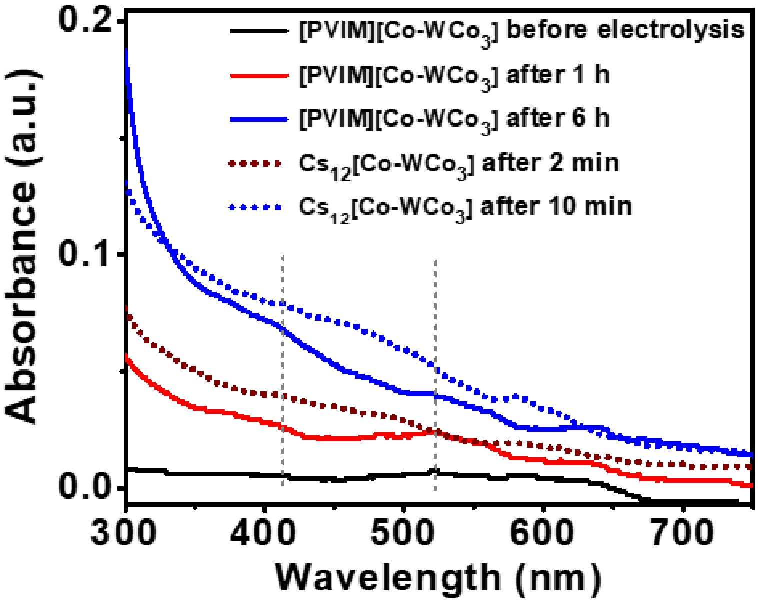

**Figure S33.** In-situ UV-vis. spectroscopy of [PVIM][Co-WCo$_3$] (solid line) and Cs$_{12}$[Co-WCo$_3$] (dotted line) composite (drop-coated on ITO) in 1 M KOH solution under long term OER.

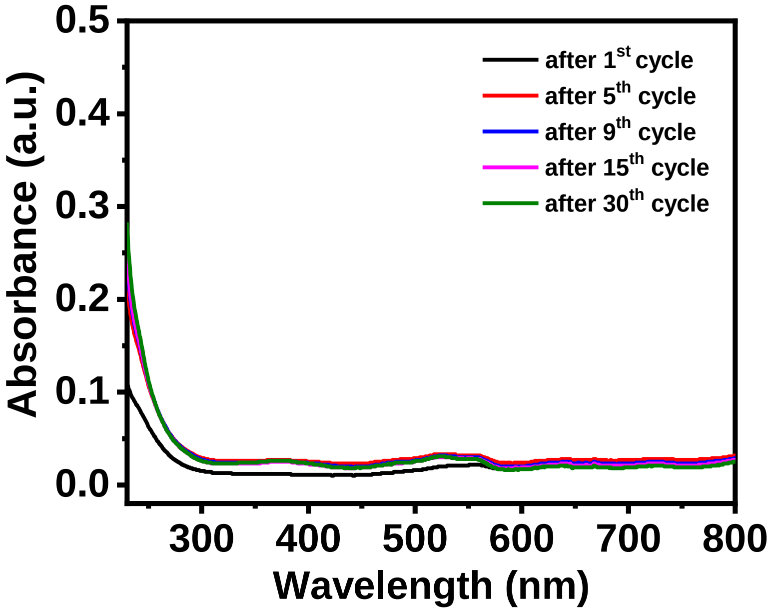

**Figure S34.** In-situ UV-vis. spectroscopy of [C$_{25}$H$_{54}$N][Co-WCo$_3$] composite (drop-coated on ITO) in 1 M KOH solution under long term OER.

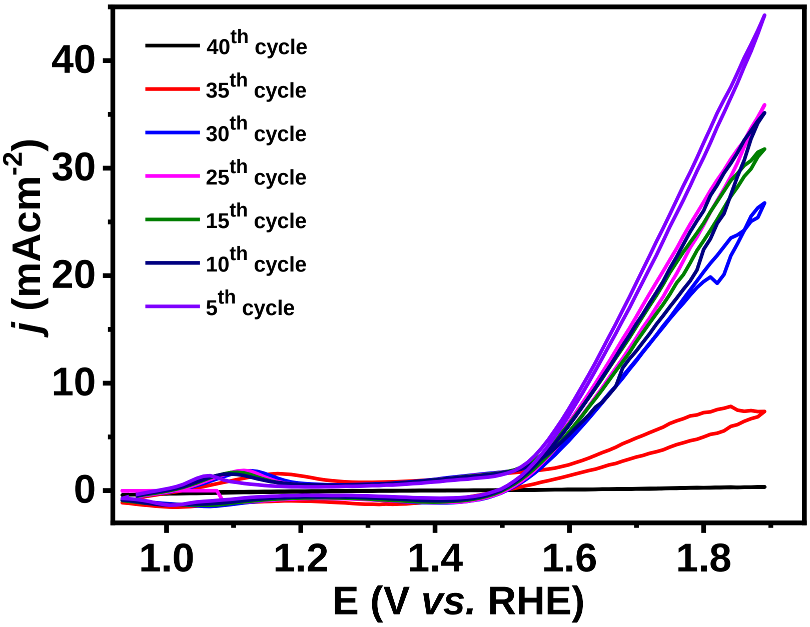

**Figure S35** Cyclic voltammogram of $Na_{12}[Co\text{-}WCo_3]$ (500 µM solution) dissolved in 1M KOH.

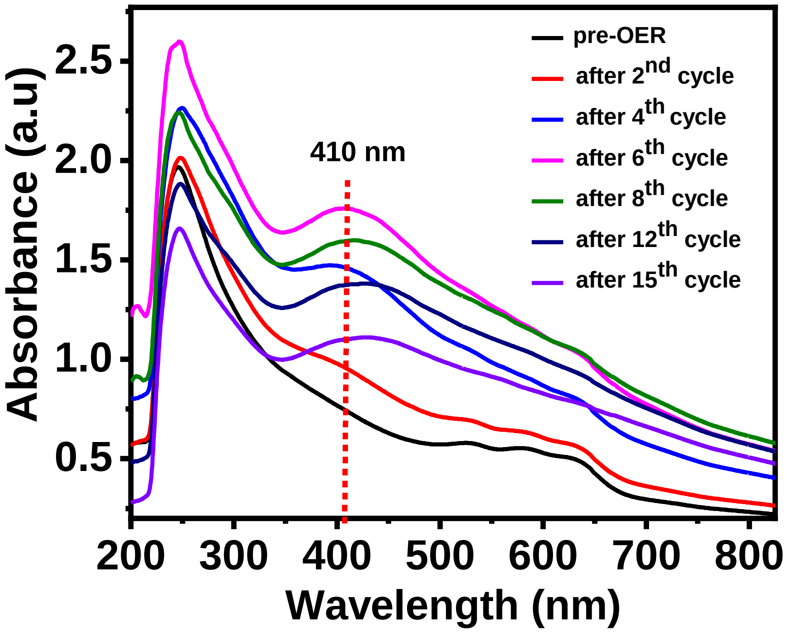

**Figure S36.** In-situ UV-vis. spectroscopy of 500 µM $Na_{12}[Co\text{-}WCo_3]$ dissolved in 1 M KOH solution (pH 14) under long term OER.

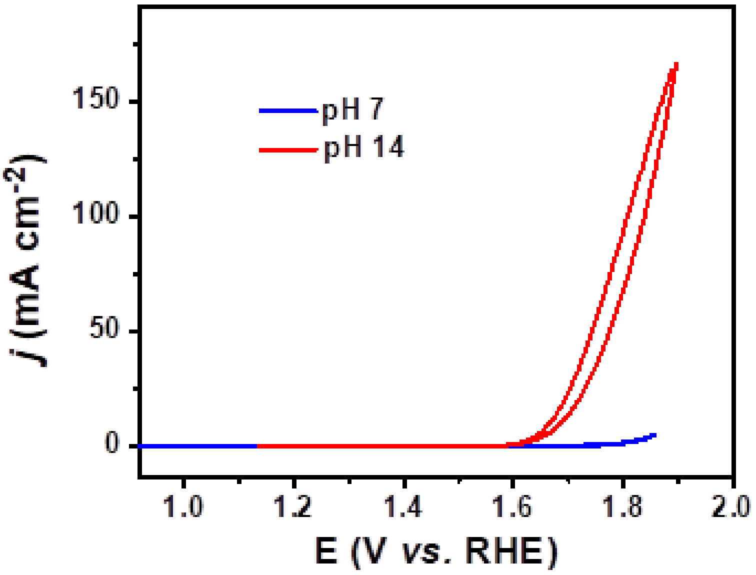

Figure S37. Cyclic voltammogram of [PVIM][V-$Co_4$] composite in (a) 0.2 M sodium phosphate buffer (pH 7) and in 1 M KOH (pH 14) at a sweep rate of 50 mV/s. CE: Pt wire; RE: Hg/HgO/1M NaOH (at pH 14) and Ag/AgCl (at pH 7).

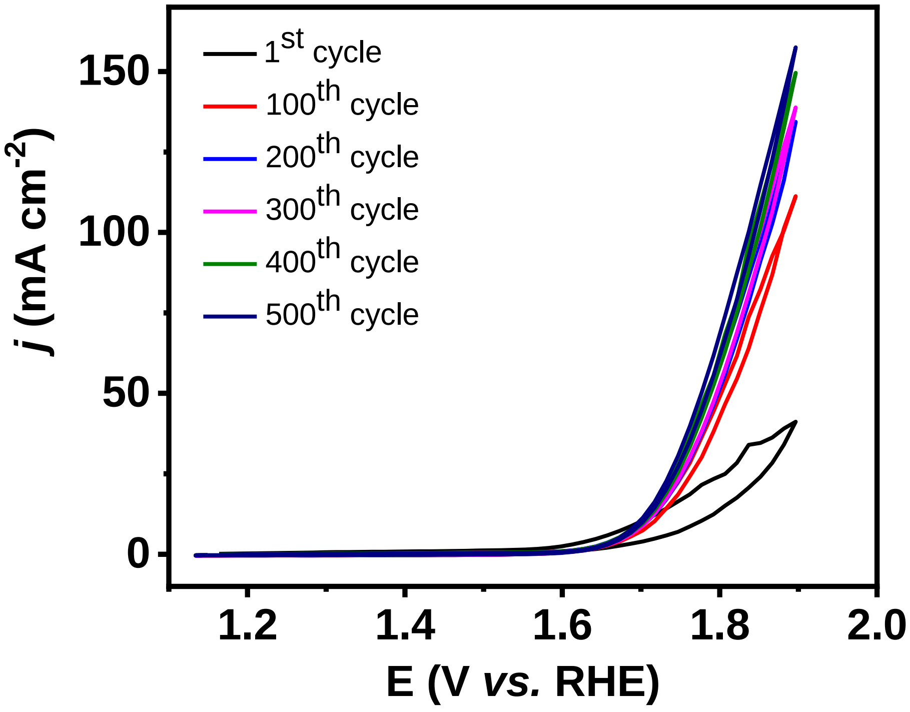

**Figure S38**. Cyclic voltammogram of [PVIM][V-$Co_4$] composite in 1 M KOH (pH 14) at a sweep rate of 50 mV/s. CE: Pt wire; RE: Hg/HgO/1M KOH.

**Table S3.** Comparison of OER by cobalt based catalysts in alkaline media

| Sl. No. | Catalyst | Reaction media (pH) | Maximum Current density ($mA/cm^2$) | Overpotential | TOF | Faradaic efficiency | Reference |
|---|---|---|---|---|---|---|---|
| 1. | $Co_3O_4$ nanocubes | 1M KOH | ~80 at 1.59 V (*vs*. RHE) | ~0.28 V at 10 $mA/cm^2$ | --- | ~97% | [7] |
| 2. | cobalt-citrate MOF | 1M KOH | ~110 at 1.95 V (vs RHE) | 0.40 V at 10 $mA/cm^2$ | --- | ~95% | [8] |
| 5. | $CoO_x$ | pH 13 | --- | <0.20 V at onset and <0.25 V at 1 $mA/cm^2$ | --- | --- | [9] |
| 6. | CoO nanoparticles on β-$Co(OH)_2$ nanosheets | Alkaline medium | --- | 0.29 V at 10 $mA/cm^2$ | --- | --- | [10] |
| 7. | Porous amorphous cobalt oxide | 1M KOH | --- | --- | 0.192/s | 95.3% | [11] |
| 8. | mixed-valence $CoO_x$ (1<x<2) | 1M KOH | 55 at 1.65 V (*vs*. RHE) | ~0.32 V at 10 $mA/cm^2$ | --- | --- | [12] |
| 10. | surface $Co^{3+}$ -rich catalyst | 1M KOH |  | 0.33 V at onset | 6.36/s |  | [13] |
| 11. | $Co(OH)_xS$ | pH 14 | --- | 0.28 and 0.36 V at 100 and 1000 $mA/cm^2$ | 0.055/s | --- | [14] |
| 13. | $Co_3O_4$ nanoparticles | pH 14 | --- | 0.31 V (at 0.5 $mA/cm^2$) | ----- | ----- | [15] |

**Table S4.** Comparison of OER by polyoxometalates based catalysts in alkaline media

| | | | | | | | |
|---|---|---|---|---|---|---|---|
| 14. | CoNi-POM@Ni Foam | 0.1M NaOH | --- | 0.36 V at 10 $mA/cm^2$ | ----- | 96% | [16] |
| 15. | $TiO_2$@[PEI ($Co_4$POM)] | 0.1M NaOH | 33.5 $mA/cm^2$ at 1.9 V *vs*. RHE | 0.49 V at 10 $mA/cm^2$ | ---- | 91% | [17] |
| 16. | $PW_{12}$@amZIF | 1M KOH | ----- | 0.31 V at 10 $mA/cm^2$ | ---- | 94.3% | [18] |
| 17. | [PVIM][$Co_4$POM] | 1M NaOH | 250 $mA/cm^2$ at 1.75 V *vs*. RHE | 0.26 V at 10 $mA/cm^2$ | 52.8/s |  | Our previous work[19] |
| 18. | [PVIM][Co-$WCo_3$] | 1M KOH | 430 $mA/cm^2$ at 1.89 V *vs*. RHE | 0.28 V at 10 $mA/cm^2$ | 6.16/s | 88.7% | This work |

## References

1. N. Thakur, S. Das Adhikary, M. Kumar, D. Mehta, A. K. Padhan, D. Mandal and T. C. Nagaiah, *ACS Omega*, 2018, **3**, 2966-2973.
2. V. Singh, S. D. Adhikary, A. Tiwari, D. Mandal and T. C. Nagaiah, *Chem. Mater.*, 2017, **29**, 4253-4264.
3. S. Mukhopadhyay, J. Debgupta, C. Singh, A. Kar and S. K. Das, *Angew. Chem. Int. ed.*, 2018, **57**, 1918-1923.
4. Q. Yin, J. M. Tan, C. Besson, Y. V. Geletii, D. G. Musaev, A. E. Kuznetsov, Z. Luo, K. I. Hardcastle and C. L. Hill, *Science*, 2010, **328**, 342-345.
5. H. Lv, J. Song, Y. V. Geletii, J. W. Vickers, J. M. Sumliner, D. G. Musaev, P. Kögerler, P. F. Zhuk, J. Bacsa and G. J. J. o. t. A. C. S. Zhu, *J. Am. Chem. Soc*, 2014, **136**, 9268-9271.
6. I. M. Mosa, S. Biswas, A. M. El-Sawy, V. Botu, C. Guild, W. Song, R. Ramprasad, J. F. Rusling and S. L. Suib, *J. Mater. Chem. A*, 2016, **4**, 620-631.
7. S. K. Singh, V. M. Dhavale, S. J. A. a. m. Kurungot and interfaces, *ACS Appl. Mater. Interfaces*, 2015, **7**, 442-451.
8. J. Jiang, L. Huang, X. Liu, L. J. A. A. M. Ai and Interfaces, *ACS Appl. Mater. Interfaces*, 2017, **9**, 7193-7201.
9. J. R. J. C. Galán-Mascarós, *ChemElectroChem*, 2015, **2**, 37-50.
10. S. Kundu, B. Malik, A. Prabhakaran, D. K. Pattanayak and V. K. J. C. C. Pillai, *Chem. Commun.*, 2017, **53**, 9809-9812.
11. X. Ji, Y. He and J. J. C. C. Liu, *Chem. Commun.*, 2019, **55**, 1797-1800.
12. A. Indra, B. Singh and A. Yadav, *J. Mater. Chem. A*, 2022, **10**, 3843-3868.
13. L. Liu, Y. Ou, D. Gao, L. Yang, H. Dong, P. Xiao and Y. J. J. o. P. S. Zhang, *J. Power Sources* 2018, **396**, 395-403.
14. H. Zhang, B. Chen, H. Jiang, X. Duan, Y. Zhu and C. J. N. Li, *Nanoscale*, 2018, **10**, 12991-12996.
15. J. D. Blakemore, H. B. Gray, J. R. Winkler and A. M. J. A. C. Muller, *ACS Catal.*, 2013, **3**, 2497-2500.
16. W. Luo, J. Hu, H. Diao, B. Schwarz, C. Streb and Y. F. J. A. C. I. E. Song, *Angew. Chem. Int. Ed.* , 2017, **56**, 4941-4944.
17. R. Gong, D. Gao, R. Liu, D. Sorsche, J. Biskupek, U. Kaiser, S. Rau and C. Streb, *ACS Appl. Energy Mater.*, 2021, **4**, 12671-12676.
18. Y. Zhao, D. Gao, S. Liu, J. Biskupek, U. Kaiser, R. Liu and C. Streb, *Chem. Eur. J.*, 2023, e202203220.
19. S. D. Adhikary, A. Tiwari, T. C. Nagaiah, D. J. A. a. m. Mandal and interfaces, *ACS Appl. Mater. Interfaces* 2018, **10**, 38872-38879.